Summer-temperature evolution on the Kamchatka Peninsula, Russian Far East, during the past 20,000 years

Vera D. Meyer[1,2], Jens Hefter[1], Gerrit Lohmann[1], Lars Max[1], Ralf Tiedemann[1] and Gesine Mollenhauer[1,2,3]

[1] Alfred Wegener Institute Helmholtz Centre for Polar and Marine Research, Bremerhaven, 27570, Germany
[2] Department of Geosciences University of Bremen, Bremen, 28359, Germany
[3] MARUM- Centre for Environmental Sciences, University of Bremen, Bremen, 28359, Germany

Correspondence to: V. D. Meyer (vera.meyer@awi.de)

Abstract. Little is known about the climate evolution on the Kamchatka Peninsula during the last glacial-interglacial transition as existing climate records do not reach beyond 12 ka BP. In this study, a summer-temperature record for the past 20 ka is presented. Branched glycerol dialkyl glycerol tetraethers, terrigenous biomarkers suitable for continental air temperature reconstructions, were analyzed in a sediment core from the western continental margin off Kamchatka in the marginal Northwest Pacific (NW Pacific). The record suggests that summer temperatures on Kamchatka during the Last Glacial Maximum (LGM) equaled modern. We suggest that strong southerly winds associated with a pronounced North Pacific High pressure system over the subarctic NW Pacific accounted for the warm conditions. A comparison with an Earth System Model reveals discrepancies between model and proxy-based reconstructions for the LGM-temperature and atmospheric circulation in the NW Pacific realm. The deglacial temperature development is characterized by abrupt millennial-scale temperature oscillations. The Bølling/Allerød warm-phase and the Younger Dryas cold-spell are pronounced events, suggesting a connection to North-Atlantic climate variability.

Key words: CBT/MBT, summer temperature, Northwest Pacific, deglaciation, atmospheric circulation

1. Introduction

During the Last Glacial Maximum (LGM; i.e. 24-18 ka BP; Mix et al., 2001), when sea level regression lead to the exposure of the Bering and Chukchi Shelves, the Bering Land Bridge connected Alaska and eastern Siberia (Fig. 1). The resulting continuous landmass is commonly known as "Beringia" (defined as the area extending from the Lena River in Northeast Russia to the lower Mackenzie River in Canada; Hopkins et al. (1982)). Beringia's environmental history since the last glaciation is of particular interest since having been unglaciated during the LGM the landmass formed a glacial refuge for arctic flora and fauna (Abbott und Brochmann, 2002; Nimis et al., 1998; Guthrie, 2001) and allowed plants, animals and humans to migrate between Asia and America (e.g. Mason et al., 2001). Despite several studies investigating the Beringian evolution of temperature, moisture availability and vegetation (e.g. Lozhkin et al., 1993; Anderson et al., 1996; Bigelow and Edwards, 2001; Bigelow and Powers, 2001; Pisaric et al., 2001; Elias, 2001; Ager, 2003; Kienast et al., 2005; Sher et al., 2005; Lozhkin et al., 2007:

Kurek et al., 2009; Elias and Crocker, 2008; Kokorowski et al., 2008a, b: Berman et al., 2001; Fritz et al., 2012; Anderson and Lozhkin, 2015) environmental change during the LGM-to-Holocene transition and the respective climatic controls (e.g. rising atmospheric CO_2-levels, insolation and regional atmospheric and oceanic circulation) remain elusive. This is because continuous terrestrial records covering the entire last glacial-interglacial transition are sparse, particularly in western Beringia (i.e. Siberia; e.g. Kokorowski et al., 2008a and references therein; Andreev et al., 2012; Anderson and Lozhkin, 2015). This is a gap of knowledge as independent terrestrial data on temperature and moisture availability are needed to infer LGM-to-Holocene changes in atmospheric circulation in the North Pacific realm (e.g. Mock et al., 1998; Kokorowski et al., 2008a) and to validate climate model outputs.

The sparsity of continuous temperature records in Beringia also limits a comprehensive assessment of the geographic extent of abrupt deglacial climate reversals. There is consensus among sea surface temperature records from the North Pacific (N Pacific) and its marginal seas that the deglaciation was characterized by abrupt warm-cold oscillations (e.g. Barron et al., 2003; Seki et al., 2009; 2014; Caissie et al., 2010; Max et al., 2012; Praetorius and Mix, 2014; Praetorius et al., 2015; Meyer et al., 2016) suggesting teleconnections with the North-Atlantic realm (Manabe and Stouffer, 1988; Mikolajewicz et al., 1997; Okumura et al., 2009; Chikamoto et al., 2012). Yet, it is not fully understood how far this North Atlantic (N Atlantic) connection extended into Beringia. Records are inconsistent suggesting both abrupt warm-cold oscillations (Anderson et al., 1990; Andreev et al., 1997; Pisaric et al., 2001; Bigelow and Edwards, 2001; Bigelow and Powers, 2001; Brubaker et al., 2001; Anderson et al., 2002; Meyer et al., 2010; Anderson and Lozhkin, 2015) and continuous warming (Lozhkin et al., 1993, 2001; Anderson et al., 1996, 2002; Lozhkin and Anderson, 1996; Bigelow and Powers, 2001; Nowaczyk et al., 2002; Ager, 2003; Anderson et al., 2003; Nolan et al., 2003; Kokorowski et al., 2008a,b; Kurek et al., 2009) throughout the deglaciation.

The Kamchatka Peninsula (attached to Siberia, Fig. 1a) is among of the areas in western Beringia where the least is known about environmental conditions during the LGM-to-Holocene transition since terrestrial archives on Kamchatka do not reach beyond 12 ka BP (e.g. Dirksen et al., 2013, 2015; Nazarova et al., 2013; Hoff et al. 2014, 2015; Klimaschewski et al., 2015; Self et al., 2015; Solovieva et al., 2015). Kamchatka is an important location to study deglacial changes in regional atmospheric and oceanic circulation in the Northwest Pacific realm. Protruding into the NW Pacific (NW Pacific: Fig. 1a) the peninsula responds to variations in these regional climate controls in addition to global or supra-regional climate drivers, e.g. summer insolation or teleconnections with the N-Atlantic realm, as has been shown for the Holocene (Savoskul, 1999; Dirksen et al., 2013; Nazarova et al., 2013; Andrén et al., 2015; Brooks et al., 2015; Hammarlund et al., 2015; Self et al., 2015).

In this study, we analyzed branched glycerol dialkyl glycerol tetraethers (brGDGTs), terrigenous biomarkers as recorders of continental air temperature (Weijers et al., 2006a, 2007), in a marine sediment core retrieved at the eastern continental margin off Kamchatka/NW Pacific (site SO201-2-12KL, NW Pacific, Fig. 1a, b). We present a continuous, quantitative record of summer-temperature for the past 20 ka and infer changes in atmospheric circulation. The findings are compared to an Earth System Model (ESM).

2. Regional Setting

The Kamchatka Peninsula is situated south of the Koryak Uplands and seperates the Sea of Okhotsk from the NW Pacific and the Bering Sea (Fig. 1a). It is characterized by strong variations in relief with lowlands in the coastal areas (Western Lowlands; Eastern Coast) and mountain ranges further inland (Fig. 1b). The mountain ranges, the Sredinny and the Eastern Ranges, encircle the lowlands of the Central Kamchatka Depression (CKD; Fig. 1b). The CKD is the largest watershed of the Peninsula and is drained by the Kamchatka River, the largest river of Kamchatka. The river discharges into the Bering Sea near 56°N (Fig. 1b). The climate is determined by marine influences from the surrounding seas, by the East Asian continent, and by the interplay of the major atmospheric pressure systems over NE-Asia and the N Pacific (e.g. Mock et al., 1998; Glebova et al., 2009). In general the climate is classified as sub-arctic maritime (Dirksen et al., 2013). The winters are characterized by cold and relatively continental conditions since northerly winds prevail over Kamchatka, mainly associated with the Aleutian Low over the N Pacific and the Siberian High over the continent (Mock et al., 1998). In summer, Kamchatka experiences warm maritime conditions owing to the East Asian Low over the continent and the North Pacific High (NPH) over the N Pacific (Mock et al., 1998). Furthermore, there are the influences of the East Asian Trough (EAT) which has its average position over the Chukchi Shelf, as well as the influences of the westerly jetstream and the associated polar front (Mock et al., 1998). Variations in the position and strength of the EAT affect precipitation and temperature over Beringia and can cause climatic contrasts between Siberia and Alaska (Mock et al., 1998 and references therein). With respect to Kamchatka westerly to northwesterly winds associated with the jetstream and the EAT form a source of continental air masses from Siberia/East Asia (Mock et al., 1998).

The mountainous terrain with strongly variable relief results in pronounced climatic diversity on the Peninsula (Fig. 1b). The coastal areas, the western Lowlands and the Eastern Coast, are dominated by marine influences. In the coastal areas, summers are cool and wet and winters are relatively mild. Precipitation is high along the coast and in the mountains throughout the year (Kondratyuk, 1974; Dirksen et al., 2013). Being protected from marine influences by the mountain ranges, the CKD has more continental conditions with less precipitation and a larger

annual temperature range than in the coastal areas (Ivanov, 2002; Dirksen et al., 2013, Kondratyuk, 1974; Jones and Solomina, 2015). Mean temperatures averaged for the entire Peninsula range from -8 to -26°C in January and from 10 to 15°C in July (Ivanov, 2002).

3. Material and Methods

3.1. Core material and chronology

Within a joint German/Russian research program (KALMAR Leg 2) core SO201-2-12KL (Fig. 1a, b) was recovered with a piston-corer device during cruise R/V SONNE SO201 in 2009 (Dullo et al., 2009). The core material was stored at 4°C prior to sample preparation. Age control is based on accelerator mass spectrometry (AMS) radiocarbon dating of planktic foraminifera (*Neogloboquadrina pachyderma* sin.; 9 dates in total) as well as on correlations of high-resolution spectrophotometric (color b*) and X-ray fluorescence (XRF) data from different sediment cores from the NW Pacific, the Bering Sea and the Sea of Okhotsk (Max et al., 2012). The correlation allowed to transfer AMS results from core to core, which provided 10 additional age control points for site 12KL (Max et al., 2012). Max et al. (2012) converted radiocarbon ages into calibrated calendar ages using the calibration software Calib Rev 6.0 (Stuiver and Reimer, 1993) with the Intcal09 atmospheric calibration curve (Reimer et al., 2009). A constant reservoir age of 900 years was assumed for the entire time-interval covered by the core. The uncertainty of AMS dating was smaller than ± 100 years (Max et al., 2012). Another important source of uncertainty are changes in reservoir ages of the surface ocean during the last deglaciation (Sarnthein et. al., 2015). However, recent studies suggest that reservoir ages of the Bering Sea and the N Pacific varied by less than 200 years (Lund et al., 2011; Kühn et al., 2014) and are within the range of reservoir ages originally assumed by Max et al. (2012).

Average Holocene, deglacial and glacial sedimentation rates are 39, 79 and 59 cm/ka, respectively, allowing for climate reconstructions on multi-centennial to millennial timescales (Max et al., 2012). For more detailed information about the stratigraphic framework and AMS-^{14}C results, see Max et al. (2012).

3.2. Lipid extraction

For this study we used the same samples as Meyer et al, (2016). These authors sampled the core in 10 cm steps providing an average temporal resolution of approximately 200 years. For GDGT analyses, freeze-dried and homogenized sediment samples (approximately 5 g) were extracted and processed according to Meyer et al. (2016).

3.3. GDGT analysis

GDGTs were analyzed by High Performance Liquid Chromatography (HPLC) and a single quadrupole mass spectrometer (MS). The systems were coupled via an atmospheric pressure chemical ionization (APCI) interface. The applied method was slightly modified from Hopmans et al. (2000). Analyses were performed on an Agilent 1200 series HPLC system and an Agilent 6120 MSD. Separation of the individual GDGTs was performed on a Prevail Cyano column (Grace, 3 µm, 150 mm x 2.1 mm) which was maintained at 30°C. After sample injection (20 µL) and 5 min isocratic elution with solvent A (hexane) and B (hexane with 5% isopropanol) at a mixing ratio of 80:20, the proportion of B was increased linearly to 36% within 40 min. The eluent flow was 0.2 ml/min. After each sample, the column was cleaned by back-flushing with 100% solvent B (8 min) and re-equilibrated with solvent A (12 min, flow 0.4 ml/min). GDGTs were detected using positive-ion APCI-MS and selective ion monitoring (SIM) of their $(M+H)^+$ ions (Schouten et al., 2007). APCI spray-chamber conditions were set as follows: nebulizer pressure 50 psi, vaporizer temperature 350 °C, N_2 drying gas flow 5 l/min and 350 °C, capillary voltage (ion transfer tube) -4 kV and corona current +5 µA. The MS-detector was set in SIM-mode detecting the following $(M+H)^+$ ions with a dwell time of 67 ms per ion: *m/z* 1292.3 (GDGT 4 + 4´ / crenarcheol + regio-isomer), 1050 (GDGT IIIa), 1048 (GDGT IIIb), 1046 (GDGT IIIc), 1036 (GDGT IIa), 1034 (GDGT IIb), 1032 (GDGT IIc), 1022 (GDGT Ia), 1020 (GDGT Ib), 1018 (GDGT Ic) and 744 (C_{46}-internal standard).

GDGTs were quantified by peak-integration and the obtained response factor from the C_{46} -standard. Concentrations were normalized to the dry weight (dw) of the extracted sediment and to total organic carbon contents (TOC). It has to be noted that the quantification should only be regarded as semi-quantitative because individual relative response factors between the C_{46}-standard and the different brGDGTs could not be determined due to the lack of appropriate standards. Fractional abundances of single brGDGTs were calculated relative to the total abundance of the all nine brGDGTs. The standard deviation was determined from repeated measurements of a lab internal standard sediment and resulted in an uncertainty of 9 % for the concentration of the sum of all nine brGDGT (ΣbrGDGT).

3.4. Temperature determination

The Cyclysation of Branched Tetraether index (CBT) and Methylation of Branched Tetraether index (MBT) were introduced as proxies for soil-pH (CBT) and mean annual air temperature (MAT, CBT/MBT) by Weijers et al. (2007). We calculated the CBT index after Weijers et al. (2007). For calculating the MBT-index we used a

modified version, the MBT' which excludes GDGTs IIIb and IIIc, and was introduced by Peterse et al. (2012). From repeated measurements of a lab-internal standard sediment extract (n=7) the standard deviation for CBT and MBT' were determined as 0.01 and 0.04, respectively. CBT and MBT'-values were converted into temperature using the global-soil dataset calibration by Peterse et al. (2012). The residual standard mean error of this calibration is 5°C (Peterse et al., 2012). The standard deviation of CBT and MBT' translates into an uncertainty of max. 0.1°C.

Although terrestrial soils are supposed to be the main source of br GDGTs (Weijers et al., 2007) brGDGT can also be produced in-situ in marine water systems (Peterse et al., 2009; Zhu et al., 2011; Zell et al., 2014) as well as in fresh water environments (Tierney, 2010; Zell et al., 2013; De Jonge et al., 2014; Dong et al., 2015). As in-situ production can bias temperature reconstructions, particularly in marine settings where the input of terrigenous GDGTs is low (Weijers et al., 2006b; Peterse et al., 2009, 2014; De Jonge et al., 2014), the contribution of terrigenous brGDGTs to the marine sediments needs to be estimated prior to any paleoclimatic interpretation of CBT/MBT'-derived temperatures. A common means to estimate the relative input of marine and terrestrial GDGTs is the BIT-index (branched and isoprenoid tetraether index) which quantifies the relative contribution of the marine-derived Crenarchaeol and terrigenous brGDGTs (Hopmans et al., 2004). The higher the BIT-value the more abundant the brGDGT relative to the Crenarchaeol and the higher the terrigenous input. BIT-values were adopted from Meyer et al. (2016) who worked on the same samples used in this study.

3.5. Climate simulations with the Earth System Model COSMOS

In order to compare inferences for atmospheric circulation during the summer months to General Circulation Model outputs, model simulations for the climate were performed with the Earth System model COSMOS for pre-industrial (Wei et al., 2012) and LGM conditions (Zhang et al., 2013). The model configuration includes the atmosphere component ECHAM5 at T31 resolution (~3.75°) with 19 vertical layers (Roeckner et al., 2006), complemented by a land-surface scheme including dynamical vegetation (Brovkin et al., 2009). The ocean component MPI-OM, including the dynamics of sea ice formulated using viscous-plastic rheology, has an average horizontal resolution of 3°x1.8° with 40 uneven vertical layers (Marsland et al, 2003). The performance of this climate model was evaluated for the Holocene (Wei and Lohmann, 2012; Lohmann et al., 2013), the last millennium (Jungclaus et al., 2006), glacial millennial-scale variability (Gong et al., 2013; Weber et al., 2014; Zhang et al., 2014), and warm climates in the Miocene (Knorr and Lohmann, 2014) and Pliocene (Stepanek and Lohmann, 2012).

External forcing and boundary conditions are imposed according to the protocol of PMIP3 for the LGM (available at http://pmip3.lsce.ipsl.fr/). The respective boundary conditions for the LGM comprise orbital forcing, greenhouse gas concentrations (CO_2=185ppm; N_2O=200ppb; CH_4=350ppb), ocean bathymetry, land surface topography, run-off routes according to PMIP3 ice sheet reconstruction and increased global salinity (+ 1 psu compared to modern value) to account for a seal level drop of ~116 m. The glacial ocean was generated through an ocean-only phase of 3000 years and coupled phase of 3000 years (LGMW in Zhang et al., 2013). The land cover is calculated interactively in the climate model which has an interactive land surface scheme and vegetation module (Brovkin et al.2009). The modular land surface scheme JSBACH (Raddatz et al., 2007) with vegetation dynamics (Brovkin et al., 2009) is embedded in the ECHAM5 atmosphere model. The background soil characteristics (which are described in Staerz et al., 2016) are set to the values which are closest to the pre-industial land points.

For both, PI and LGM conditions, the climate model was integrated twice for 3000 model years and provides monthly output (Wei et al., 2012; Wei and Lohmann, 2012; Zhang et al., 2013). . Here, anomalies in sea-level pressure (SLP), wind directions (1000 hPa level) and surface air temperature (SAT) between the LGM and pre-industrial conditions were analyzed for the boreal summer season - June, July and August (JJA). We focus on the summer season as in high latitudes brGDGTs seem to reflect summer temperature instead of the annual mean (Rueda et al., 2009, Shannahan et al., 2013; Peterse et al., 2014). All produced figures show climatological mean characteristics averaged over a period of 100 years at the end of each simulation.

4. Results

4.1. Concentrations and fractional abundances of brGDGTs

The summed concentration of all nine brGDGTs (ΣbrGDGT) is shown in Figure. 2a. The concentration of ΣbrGDGTs vary between 40 and 160 ng/g dw throughout the record. Ranging between 60-80 ng/g dw, they are lowest during the LGM and the late Holocene. During the deglaciation and the early Holocene (17-8 ka BP) lowest values are approximately 80 ng/g dw, except for two peaks at 15-16 ka BP and 12-13 ka BP, respectively, where concentrations reach ~160 ng/g dw (Fig. 2a).

The fractional abundance of all nine brGDGTs, calculated relative to the ΣbrGDGT, is shown in Figure. 3. All samples are characterized by a similar pattern. The composition of the brGDGT assemblage is dominated by brGDGTs without cyclopentyl moieties which together account for 60-80% of the total brGDGT-assemblage

(GDGT Ia, IIa, IIIa; Fig. 3). brGDGTs with a higher degree of methylation are more abundant than lesser methylated ones. In 88 out of 92 samples GDGT IIIa is the most prominent brGDGT accounting for 22-37% of the total brGDGT distribution. It is closely followed by GDGT IIa with 16-29% and GDGT Ia which accounts for 14-23% of the total brGDGT assemblage. As for brGDGTs containing cyclopentyl moieties, GDGT IIb is most abundant accounting for 9-16% of the total brGDGT assemblage. GDGT IIc, Ib, Ic, IIIb and IIIc are less abundant reaching 2-6%, 3-7%, 1-3%, 2-4%, and 1-2%, respectively. (Fig. 3).

4.2. Temperature development over the past 20 ka

The CBT/MBT'-derived temperatures are plotted in Fig. 2b. Glacial (20-18 ka BP) and late Holocene (1-3 ka BP) temperatures are the similar (~7.5°C). (Fig. 2b). The deglaciation is characterized by abrupt temperature variations. At 18 ka, temperature drops by ~1.5°Cand remains relatively cold until approximately 14.6 ka BP, where it abruptly jumps back to the glacial and Holocene level of ~7.5°C (Fig. 2e). Between ~14.6 and ~13 ka, temperature progressively decreases ~1-0.5°C. Temperature abruptly decreases by ~2°C at approximately 13 ka BP and remains cold until 12 ka BP (Fig. 2b). The cold spell is followed by a sharp temperature increase of ~3°C at the onset of the Preboreal (PB)/early Holocene (Fig. 2b). After the abrupt temperature increase into the PB temperature progressively increases culminating in a Mid-Holocene Thermal Maximum (HTM) between ~8 and~4-5 ka BP where temperatures ranges between ~7.5-8°C (Fig. 2b). .

4.3. LGM-climate simulation with COSMOS

4.3.1. Sea-level pressure and wind patterns

Model-simulations for SLP (JJA) are shown Fig. 4a. The LGM-simulation is characterized by strong positive anomalies in sea-level pressure (SLP) over the North American Continent (Fig. 4a). Positive SLP-anomalies also occur over the Arctic Ocean. Negative SLP anomalies occur south of 50°N and are centered over the NW Pacific and East Asia, but are also observed in a few grid-cells over the central and NE Pacific and over the Sea of Okhotsk. In the Bering Sea, the northern N-Pacific (north of 50°N) and Beringia SLP does not change significantly relative to present.

The positive SLP-anomalies over North America are associated with pronounced anticyclonic anomalies in the wind directions, which expand to the Chukchi-Sea and to the formerly exposed Bering Land Bridge (Fig. 4a). Over western Beringia as well as the adjacent Arctic Ocean small northerly anomalies are present. Between 100°E and 110°E pronounced anticyclonic anomalies are present over Russia. Over Kamchatka and the adjacent East Siberian

Coast small northerly anomalies occur. The western Bering Sea is characterized by easterly anomalies. Over the NW Pacific anomalies are small and show no general pattern. In the NE Pacific relatively strong westerly to southwesterly anomalies are present.

4.3.2. Surface air temperature

Model simulations for SAT (JJA) are shown in Fig. 4b. The model predicts widespread negative surface air temperature (SAT)-anomalies over Beringia, East Asia, North America, the Arctic Ocean and the entire N Pacific (Fig. 4b). However, in small parts of the formerly exposed Bering Land Bridge slightly warmer-than-present conditions occur. On the arctic shelf there is a small band where temperature is similar to the PI-conditions (the SAT anomaly falls in the window of -1 to +1°C). The temperature anomalies are strongest over North America where they reach -17°C. Over western Beringia the SAT anomaly becomes more pronounced from east to west with SAT ranging between -1 and -5 over East Siberia and between -5 and -9 further west. Over the N Pacific SAT anomalies are smaller than over western Beringia and range between -1 and -5°C. SAT anomalies are smallest in the Bering Sea and along the eastern coast of Kamchatka. Over the Peninsula itself, the majority of grid-cells indicate a negative anomaly (-3 to -5°C). In the northern part and over the adjacent Bering Sea the SAT anomalies are very small within the window of -1 to +1°C (Fig. 4b).

5. Discussion

5.1. Sources of brGDGT and implications for CBT/MBT'-derived temperatures

Considering that brGDGT are thought to be synthesized by terrestrial bacteria which thrive in peats and soils (e. g. Weijers et al., 2006b) it is most likely that the major origin of brGDGT in the marine sediments of the Bering Sea/NW Pacific would be the Kamchatka Peninsula. However, BIT-values from core 12KL range between 0.08 and 0.2 (Meyer et al., 2016) throughout the entire record, indicating that marine derived GDGT dominate the total GDGT composition and that terrigenous input is low (Fig. 2c). Marine settings where terrigenous input is low are particularly sensitive to bias from in-situ production (e.g. Weijers et al., 2006b; Peterse et al., 2009; Zhu et al., 2011), thus non-soil derived brGDGTs potentially have a considerable effect on the temperature reconstruction at site 12KL. However, the concentrations of ΣbrGDGT show similarities with the trend of Titanium/Calcium ratios (Ti/Ca-ratios, Fig. 2d) from core 12KL (XRF-data from Max et al. (2012)). Ti/Ca-ratios reflect the proportion of terrigenous and marine derived inorganic components of the sediment, and can be used as an estimator of terrigenous input. With relatively high values at 15.5 and 12 ka BP, and minima at 14 and 11 ka BP Ti/Ca indicates

relatively high contributions of terrigenous material relative to marine components at 15.5 and 12 ka BP and relatively low terrigenous contributions at 14 and 11 ka BP. A similar pattern is visible in ΣbrGDGT-concentrations as these increase during intervals of enhanced terrigenous input (high Ti/Ca-values) and decrease when terrigenous input is relatively low (low Ti/Ca values, see Fig. 2b, d). This suggests that brGDGTs are terrigenous.. Moreover, the distribution of the brGDGTs the samples from site 12KL resemble the brGDGT composition described for soils world-wide (Weijers et al., 2007; Blaga et al., 2010) as GDGT Ia, IIa and IIIa dominate over brGDGTs with cyclopentyl moieties (e.g. Ib, IIb) accounting for 60-80% of the total brGDGT assemblage (Fig. 3). By contrast, in marine areas where brGDGTs are thought to be produced in-situ, the brGDGT compositions were dominated by brGDGTs containing cyclopentyl moieties (Peterse et al., 2009; Zell et al., 2014). Thus, brGDGT seem to be soil-derived and a bias from in-situ production is unlikely. We also exclude changes in the source of brGDGTs through time because the relative abundance of the brGDGTs is similar in all samples indicating that the source of brGDGTs remained constant throughout the past 20 ka (Fig. 3). We consider the catchment of the Kamchatka River (CKD and inner flanks of the mountains) and the Eastern Coast as the likely sources of brGDGTs deposited in the marine sediments at the core site since the Kamchatka River and several small rivers draining the Eastern Coast discharge into the western Bering Sea. Flowing southward along Kamchatka, the East Kamchatka Current would carry the load of the Kamchatka River to site 12KL (Fig. 1b)

Although the CBT/MBT-paleothermometre has been suggested to generally record mean annual air temperatures (Weijers et al., 2007) it is assumed to be biased to the summer months/ice-free season in high latitudes (Rueda et al., 2009, Shannahan et al., 2013; Peterse et al., 2014). According to Klyuchi climate station (for location see Fig. 1b), mean annual air temperatures in the northern CKD are -0.5°C (http://en.climate-data.org/location/284590/). The CBT/MBT'-derived temperatures for the core-top/late Holocene (7.5 ± 5°C; Fig. 2) exceed the annual mean by .~8°C and are similar to mean air temperatures from the ice-free season (May-October) at Klyuchi (9°C). Therefore, they are interpreted as summer temperature and will be referred to as "Mean Air Temperature of the ice-free season" (MAT_{ifs}) henceforth.

5.2. Temperature evolution over the past 20 ka

5.2.1. The LGM (until 18 ka)

The finding that LGM summers were as warm as duringthe Holocene contrasts with the general understanding of the glacial climate, according to which the extratropics were significantly colder than today, as documented by several proxy-based temperature reconstructions and general circulation model simulations (e.g. MARGO

compilation or PIMP, and others; see Kutzbach et al., 1998; Kageyama et al., 2001; Kageyama et al., 2006; Kim et al., 2008; Braconnot et al., 2012; Alder and Hostetler, 2015). Generally cooler LGM temperatures are thought to result from low summer insolation, reduced carbon-dioxide concentrations in the atmosphere and extensive continental ice sheets (Berger and Loutre 1991; Monnin et al., 2001; Kageyama et al., 2006, Shakun et al., 2012).

295 Therefore, one may expect that the Kamchatka Peninsula would experience a glacial-interglacial warming trend. As MAT_{ifs} deviates from the trends in atmospheric CO_2 (CO_{2atm}) and insolation (Fig. 2b, e, f) regional climate drivers may have overprinted the effects of CO_{2atm} and summer insolation. Interestingly, several studies investigating climate in Beringia based on pollen and beetle-assemblages indicate that in NE Siberia and the formerly exposed Bering Land Bridge (catchments of the Lena, Kolyma and Indigirka Rivers, Ayon Island, Anadyr

300 Lowlands, Lake El'Gygytgen, Seward Peninsula, Fig. 4c) summers during the LGM were as warm as at present or were even warmer (Fig. 4c; Elias et al., 1996, 1997; Elias, 2001; Alfimov and Berman, 2001; Kienast, 2002; Kienast et al., 2005; Sher et al., 2005; Berman et al., 2011). Only a few pollen and insect data from Markovo, Jack London and Lake El'Gygytgyn Lakes (Fig. 1a), point to colder-than-present summer conditions (Fig. 4c; Lozhkin et al., 1993; Alfimov and Bermann, 2001; Lozhkin et al., 2007; Pitul'ko et al., 2007). The fairly large number of

305 sites indicating warm summers in Siberia suggests that a thermal anomaly was widespread over western/central Beringia (Fig. 4c) and extended to Kamchatka. The thermal anomaly did probably not extend to eastern Beringia as insect-data as well as pollen consistently point to summer cooling of up to 4°C (Fig. 4c; e.g. Mathews and Telka, 1997; Elias, 2001; Kurek et al., 2009).

5.2.2. Regional controls on MAT_{ifs}

310 In previous studies the warm Siberian summers during the LGM were attributed to increased continentality, which would arise from the exposure of the extensive Siberian and Chukchi shelves at times of lowered sea-level (Fig. 1a; e.g. Guthrie, 2001; Kienast et al., 2005; Berman et al., 2011). The greater northward extent of the Beringian landmass (approximately +800 km relative to today) would have minimized maritime influences from the cold Siberian and Chukchi Seas (Guthrie, 2001; Alfimov and Berman, 2001; Kienast et al., 2005; Sher et al., 2005;

315 Berman et al., 2011). Increased seasonal contrasts resulting in warmer summers and colder winters would have been the result (e.g. Guthrie, 2001; Kienast et al., 2005). Winter cooling in Siberia (relative to modern) is indicated by ice-wedge data (Meyer et al., 2002) from Bykovski Peninsula (Fig. 1a). Also, the presence of stronger-than-present sea-ice cover in the Bering Sea (Caissie et al., 2010; Smirnova et al., 2015) points to cold winters in Siberia and Kamchatka during the LGM. However, for Kamchatka it is unlikely that the thermal anomaly and an increased

320 seasonal contrast were a direct result from lowered sea-level as the bathymetry around the Peninsula is relatively

steep and the exposed shelf area was very small. (Fig. 1a, b). Thus, other climate drivers were likely responsible for the relatively warm summer conditions. Potential mechanisms are changes in oceanic or atmospheric circulation.

Intriguingly, $U^{K'}_{37}$-based SST reconstructions from the Sea of Okhotsk indicate that glacial SST were slightly warmer than today or equal to modern conditions (Seki et al., 2004, 2009; Harada et al., 2004, 2012; Fig. 4c). However, these records are considered to be biased by seasonal variations in the alkenone production rather than to reflect real temperature anomalies (Seki et al., 2004, 2009; Harada et al., 2004, 2012). This seems to be supported by a few TEX^{L}_{86}-based SST reconstruction from the Sea of Okhotsk suggesting that LGM SST were ~5°C colder than at present (Seki et al. 2009; 2014). In this light, a climatic relation between alkenone-based SST and MAT_{ifs} seems very unlikely. Interestingly, LGM-SST in the subarctic NW Pacific (site 12KL, TEX^{L}_{86}) were only ~1°C lower than at present (Fig. 2 h), a relatively small temperature difference compared to other SST records from the NW Pacific and its marginal seas (all obtained from TEX^{L}_{86}) which suggest a cooling of ~4-5°C (e.g. Seki et al., 2009; 2014; Meyer et al., 2016). The relatively warm SST at site 12KL were explained by a stronger-than-present influence of the Alaskan Stream in the marginal NW Pacific (Meyer et al., 2016). Such warm SST may have supported the establishment of warm conditions on Kamchatka. However, it is unlikely, that the temperature development on Kamchatka was fully controlled by oceanic influences since this would probably have caused a reduction of LGM MAT_{ifs} relative to present.

If oceanic circulation alone is unlikely to have caused the warm temperatures on Kamchatka, atmospheric circulation may have exerted an important control on glacial summer temperatures in the region. In terms of atmospheric circulation the summer climate of the Kamchatka is largely determined by the strength and position of the North Pacific High (NPH) over the N Pacific (Mock et al., 1998). As the southerly flow at the southwestern edge of the NPH brings warm and moist air masses to Kamchatka summers on the Peninsula become warmer when the NPH and the associated warm southerly flow increase in strength (Mock et al., 1998). This modern analogue suggests that the LGM-NPH over the subarctic NW was stronger than today and the resulting warming effect may have balanced the cooling effects of CO_{2atm} and insolation.

5.2.2.1. Comparison to the COSMOS-simulations

These inferences contrast with results from the climate simulations with COSMOS. For JJA the model predicts a decrease in SLP over the NW-Pacific suggesting that the southerly flow at the western edge of the NPH was

reduced rather than strengthened (Fig. 4a). The weakening of the southerly flow is also discernable in the anomaly of the major wind-patterns over the NW Pacific (Fig. 4a) as a small northerly anomaly occurs north of Kamchatka, over the Peninsula itself and along the Asian coast (Fig. 4a). The weakening of the NPH is agreement with several other General Circulation Model (GCM), which consistently predict a reduction in SLP over the N-Pacific (Kutzbach and Wright, 1985; Bartlein et al., 1998; Dong and Valdes, 1998; Vetteoretti et al., 2000; Yanase and Abe-Ouchi, 2007; Alder and Hostetler, 2015). It has been suggested that a pronounced positive SLP-anomaly and a persistent anticyclone over the American continent resulted in reduced SLP over the Western North Pacific (Yanase and Abe Ouchi, 2010). The positive SLP-anomaly and the strong anticyclonic tendencies are clearly present in the COSMOS simulation of SLP and wind-patterns (Fig. 4a) and were also simulated by several other GCMs (e.g. Yanase and Abe-Ouchi, 2007; 2010; Alder and Hostetler, 2015). Its development was attributed to the presence of extensive ice sheets on the American continent (Yanase and Abe-Ouchi, 2010), which would have caused severe cooling of the overlying atmosphere. Considering the consistency of different GCMs, the anticyclonic anomalies over North America as well as resulting cyclonic anomalies over the N-Pacific seem to be a robust feature of the glacial atmospheric circulation. Therefore, it is unlikely that the increased influence of the NPH over Kamchatka (as inferred from MAT_{ifs}) was caused by a general strengthening of the NPH. We hypothesize that the NPH may have weakened in response to strong anticyclonic anomalies over the LIS but at the same time shifted westward relative to today. Since the NPH is centered over the NE Pacific under present-day conditions a westward shift would automatically increase the strength of the southerly flow over the NW Pacific. This may explain why the influence of the NPH became stronger over the NW Pacific despite a general weakening of the anticyclone.

Interestingly, the general patterns of temperature change over Beringia and the N Pacific Ocean (as inferred from the proxy compilation, Fig. 4c) suggests that the LGM thermal gradient between western/central Beringia and the N-Pacific Ocean was increased relative to today (Fig. 4c). While warm summers were widespread in western Beringia (Alfimov and Berman, 2001; Kienast, 2002; Kienast et al., 2005; Sher et al., 2005; Berman et al., 2011), the majority of SST records from the open N Pacific and the Bering Sea indicate colder conditions during the LGM (Fig. 4c; deVernal and Pedersen, 1997; Seki et al., 2009, 2014; Kiefer and Kienast, 2005; Harada et al., 2004; 2012; Maier et al., 2015; Meyer et al., 2016). Under the assumption that alkenone-based reconstructions of LGM SST in the Sea of Okhotsk (Seki et al., 2004, 2009; Harada et al., 2004, 2012) are biased, also the Sea of Okhotsk may have been significantly colder than at present as suggested by TEX^{L}_{86}-based SST reconstruction (reduced by ~4-5°C Seki et al. 2009; 2014). An increased thermal gradient between the subarctic N Pacific and western

Beringia would translate into an increased pressure gradient betweenland and ocean which would intensify the southerly flow over the Kamchatka relative to today. Combined with a weakening of the NPH over the NE Pacific (due to American ice sheets) this mechanism may have been a potential cause for the westward shift of the NPH.

The distribution of temperature anomalies in the COSMOS simulation shows a different pattern than the proxy compilation (Fig. 4b and c). The model predicts a widespread cooling over Siberia and Kamchatka where the majority of proxy data suggests warmer or equal temperatures relative to present. Relatively warm summers in western and central Beringia (as inferred from the proxy data) have been explained by increased continentality due to the exposure of the Siberian, Bering and Chukchi Shelfs during the LGM (Guthrie, 2001; Kienast et al., 2005; Berman et al., 2011). In the model the impact of continentality may be comparable to the proxy world over the eastern Siberian and the northern Chukchi Shelf since SAT anomalies are between -1 and +1°C (Fig. 4b) implying summer SAT similar to PI conditions. Also, positive anomalies over parts of the Bering and Chukchi Shelf are likely associated with the shelf exposure (Fig. 4b). However, for the latter, easterly to southeasterly wind anomalies over south Alaska and the Bering Land Bridge (Fig. 4b), may also play a role. Given the discrepancies between model and proxies for SAT in the Siberian interior it seems that the effect of continentality in the COSMOS simulation is weaker than in the proxy world and that other factors are more influential. Reduced CO_{2atm} is a prominent cause for lowered temperature during the LGM (e.g. Kageyama et al., 2006; Shakun et al., 2012). Furthermore, cooling over the Arctic Ocean combined with northerly anomalies in the wind patterns over the East Siberian Sea (Fig. 4b) may have enhanced the advection of cold arctic air masses to Siberia, a mechanism supporting SAT decrease in Siberia (Mock et al., 1998). Similarly, northerly anomalies are also present over Kamchakta (Fig. 4a) which are in accordance with summer cooling on the Peninsula (Fig. 4a).

Given the discrepancies between proxy-based temperature reconstructions for Siberia and the ESM, the thermal gradient between western Beringia and the subarctic NW Pacific may also differ. In the model simulation the thermal contrast between land and ocean tends to become smaller since the negative temperature anomaly over western Beringia for the most part is more pronounced than over the subarctic N-Pacific (Fig. 4b). This contrasts with the proxy compilation according to which the thermal gradient may have been increased relative to present (Fig. 4c). As the model predicts a reduction of the thermal gradient the preconditions for the increased landward air-flow are not given. In contrast a reduced thermal gradient would support a northerly anomaly, which is in accordance with the simulated wind-patterns over Kamchatka (Fig. 4a). Hence, the discrepancies between proxies and model-outputs concerning glacial summer temperature over western Beringia potentially explain the mismatch between model and proxy based reconstructions of the atmospheric circulation patterns over the NW Pacific.

5.2.3. The deglaciation (18 ka-10 ka BP)

The deglacial millenneial-scale variability resembles the climate development in the N-Atlantic as MAT_{ifs} follows the deglacial oscillations recorded in the NGRIP-$\delta^{18}O$ (Fig. 2b, i), particularly after ~15 ka BP. MAT_{ifs} mirrors the Bølling/Allerød (B/A)-interstadial, the Younger Dryas (YD)-cold reversal and the subsequent temperature increase into the Preboreal (PB; Fig. 2b, i). This similarity to N-Atlantic climate change is in line with the majority of SST-records from the surrounding seas (Ternois et al., 2000; Seki et al., 2004; Max et al., 2012; Caissie et al., 2010; Praetorius and Mix, 2014; Praetorius et al., 2015; Meyer et al., 2016). This in-phase variability between Greenland and N Pacific records is assumed to result from atmospheric teleconnections between the N-Atlantic and the N-Pacific Oceans (e.g. Manabe and Stouffer, 1988; Mikolajewicz et al., 1997; Vellinga and Wood, 2002; Okumura et al., 2009; Chikamoto et al., 2012; Max et al., 2012; Kuehn et al., 2014; Praetorius and Mix, 2014). While atmospheric coupling with the N-Atlantic seem to have affected Kamchatka between ~15 and ~10 ka BP such connection is questionable during Heinrich Stadial 1 (HS1). The cold-spell between ~18 ka BP and ~14.6 ka BP in the MAT_{ifs} record may coincide with the HS1 in the N-Atlantic but initiates 2 ka earlier than in NGRIP-$\delta^{18}O$. Therefore, the event in MAT_{ifs} is probably not associated with climate change in the N-Atlantic (Fig. 2b, g). This temporal offset cannot be explained by age-model uncertainties in core 12KL since these are in the range of a few hundred years (Max et al., 2012).If the cooling was not associated with climate change in the N-Atlantic, it could perhaps represents a local event on Kamchatka, and potentially western Beringia, marking the abrupt end of the warm LGM-conditions. Since, to the knowledge of the authors, such an event is not reported in the terrestrial realm of western Beringia, it is difficult to identify the driving processes. One may speculate that the southerly flow abruptly weakened over Kamchatka.

While the Western Bering Sea was likely coupled to the N Atlantic already prior to 15 ka BP, the NE Pacific (Praetorius and Mix, 2014) and marginal NW Pacific became linked at ~15.5 ka BP (Praetorius and Mix, 2014; Meyer et al., 2016). In the NE Pacific this was explained by a southward shift of the westerly Jet over America (Praetorius and Mix, 2014). In the marginal NW Pacific accumulation of Alaskan Stream waters likely overprinted the effect of the atmospheric teleconnection by linking the western and the eastern basins of the N Pacific (Meyer et al., 2016). Hence, the effect of the Alaskan Stream may have also determined temperature evolution on Kamchatka during the early deglaciation, which would explain why the linkage to the North Atlantic initiated around 15 ka BP.

The presence of a YD cold reversal on Kamchatka is in agreement with palynological data from Lakes Dolgoe, Smorodynovoye, Ulkhan Chabyda and Lake El'Gygytgyn (Fig. 1a; Pisaric et al., 2001; Anderson et al., 2002, Kokorowski et al., 2008a) suggesting that the N-Atlantic climate signal was transmitted to these sites (Kokorowski et al., 2008a). By contrast, a climatic reversal equivalent to the YD is often absent in records from northeast Siberia Lake Jack London, Lake Elikchan 4; Lake El'Gygytgyn and Wrangel Island (Fig. 1a; Lozhkin et al., 1993, 2001, 2007; Lozhkin and Anderson, 1996; Nowaczyk et al., 2002; Nolan et al., 2003, Kokorowski et al., 2008a,b; Andeev et al., 2012),. Compiling deglacial records from Beringia Kokorowski et al. (2008a) identified an east-west gradient across western Beringia with a YD-like climatic reversal being present west of 140°E but absent in records east of 140°E. This east-west gradient was explained by a westward shift of the East Asian Trough (EAT; today situated over the Chukchi Shelves; Mock et al., 1998) which caused cooling west of 140°E by enhancing cold northerly winds, and together with an anticyclone over the Beaufort Sea brought warming through stronger easterlies into the region east of 140°E (Kokorowski et al., 2008a). The presence of a YD-cold reversal on Kamchatka implies that the southeastern edge of Siberia was probably not affected by the shifting EAT. Several general circulation models investigating the nature of teleconnections between the N-Atlantic and N-Pacific realms suggest that the westerly jet played an important role by acting as heat-conveyor between the N-Atlantic and the N-Pacific-Oceans (e.g. Manabe and Stouffer, 1988; Okumura et al., 2009). Considering the modern average position of the westerly Jet (between 30 and 60°N) Kamchatka likely received the YD-cold reversal through the westerlies. Together with a shift of the EAT, (Kokorowski et al. 2008a), this may explain north-south differences in northeast Siberia.

5.2.4. The Holocene

Although not quite pronounced in magnitude, the long-term MAT_{ifs} evolution during the Holocene is characterized by a mid-Holocene Thermal Maximum (HTM) between ~8 and ~4-5 ka BP (Fig. 2b). Since core 12 KL a relatively poor density of age control points during the Holocene (Fig. 2b) the timing of Holocene climate change has to be interpreted with appropriate caution. Nevertheless, the timing of the HTM is in agreement with existing climate records from central and southern Kamchatka where diatom and pollen-based records indicate warm and wet conditions between 8 and 5.2 ka BP, which are associated with the HTM (Dirksen et al., 2013; Hoff et al., 2015; Brooks et al., 2015). As already discussed in previous studies this long-term temperature development is thought to respond to changes in mean summer insolation (Brooks et al., 2015 and references therein).

6. Summary and Conclusion

Based on the CBT/MBT'-paleothermometre a continuous LGM-to-late Holocene record of summer-temperature in Kamchatka is presented.

LGM-summers were as warm as at present. The warm summers may result from stronger-than-present southerly winds over Kamchatka as a result of a stronger-than-present anticyclone over the subarctic NW Pacific. The temperature reconstruction as well as the inferences for atmospheric circulation contrasts with model simulations, which predict widespread cooling over Siberia and Kamchatka, and a weakening of the NPH over the NW Pacific together with a reduction of southerly winds over Kamchatka. These discrepancies underline the need of further investigations of the LGM-climate in the NW Pacific realm using environmental indicators and GCMs.

Abrupt millennial-scale fluctuations characterize the deglacial temperature development and represent the most prominent changes in summer temperature during the past 20 ka. A first abrupt cooling-event at 18 ka BP marks the end of the warm LGM conditions and is likely caused by regional climate change, the origin of which cannot be identified, yet. From around 15 ka onwards the temperature variations seem to be linked to climate change in the N-Atlantic, presumably via atmospheric teleconnections, as the B/A-interstadial and the YD cold reversal are present. Discrepancies with northeast Siberian records are possibly related to the position of the westerly Jet.

Acknowledgments

The study was part of a Ph.D. project funded by the Helmholtz association through the President's Initiative and Networking Fund and is supported by GLOMAR – Bremen International Graduate School for Marine Sciences. Core SO201-2-12KL was recovered during cruise SO201-2 which took place in 2009 within the frame of the German-Russian research project "KALMAR" – Kurile-Kamchatka and Aleutian Marginal Sea Island Arc Systems: Geodynamic and Climate Interaction in Space and Time". We thank the Master and the crew of R/V SONNE for their professional support during the cruise. Dirk Nürnberg is thanked for providing sample material. Alexander Weise is acknowledged for his assistance on the geochemical sample preparation in the laboratories at the University of Bremen. We are grateful to two reviewers for their detailed and constructive reviews. The biomarker data obtained in this study are available at: https://doi.org/10.1594/PANGAEA.870592.

References

Ager, T.A.: Late Quaternary vegetation and climate history of the central Bering land bridge, St. Michael island, western Alaska. Quat. Res. 60, 19-32, 2003.

Alder, J. R., Hostetler, S. W. and Sciences, A.: Global climate simulations at 3000-year intervals for the last 21 000 years with the GENMOM coupled atmosphere – ocean model, Clim. Past, 11, 449–471, doi:10.5194/cp-11-449-2015, 2015.

Alfimov, A. V. and Berman, D. I.: Beringian climate during the Late Pleistocene and Holocene, Quat. Sci. Rev., 20(1-3), 127–134, doi:10.1016/S0277-3791(00)00128-1, 2001.

Anderson, P. M., Edwards, M. E., Brubaker, L. B.: Results and Paleoclimate implications of 35 years of paleoecological research in Alaska, Development in Quaternary Science 1, 427–440, 2003.

Anderson, P. M., Lozhkin, A. V., Brubaker, L. B.: A lacustrine pollen record from North Priokhot'ya: new information about late Quaternary vegetational variations in western Beringia, Arctic Alpine Res., 28, 93–98, 1996.

Anderson, P. M., Lozhkin, A. V., Brubaker, L. B.: Implications of a 24000-yr palynological record for a Younger Dryas cooling and for boreal forest development in northeastern Siberia, Quat. Res. 57, 325–333, 2002.

Anderson, P. A., and Lozhkin, A. V.: Late Quaternary vegetation of Chukotka (Northeast Russia), implications for Glacial and Holocene environments of Beringia, Quat. Sci. Rev., 107, 112-128, 2015.

Anderson, P. M., Reanier, R. E., Brubaker, L. B.: A 14000-year pollen record from Sithylemenkat Lake, north-central Alaska. Quat. Res., 33, 400–404, 1990.

Andrén, E., Klimaschewski, A., Self, A. E., Amour, N. St., Andreev, A. a., Bennett, K. D., Conley, D. J., Edwards, T. W. D., Solovieva, N. and Hammarlund, D.: Holocene climate and environmental change in north-eastern Kamchatka (Russian Far East), inferred from a multi-proxy study of lake sediments, Glob. Planet. Change, 134, 41–54, doi:10.1016/j.gloplacha.2015.02.013, 2015.

Andreev, A. A., Klimanov, V. A. and Sulerzhitsky, L. D.: Younger Dryas pollen records from central and southern Yakutia, Quat. Int., 41/42, 111–117, 1997.

Andreev, A. A., Morozova, E., Fedorov, G., Schirrmeister, L., Bobrov, a. a., Kienast, F., and Schwamborn, G.: Vegetation history of central Chukotka deduced from permafrost paleoenvironmental records of the El'gygytgyn Impact Crater. Climate of the Past, 8(4), 1287–1300. http://doi.org/10.5194/cp-8-1287-2012, 2012.

Barron, J. A., Heusser, L., Herbert, T., and Lyle, M.: High-resolution climatic evolution of coastal northern California during the past 16,000 years. Paleoceanography, 18(1), 1020, http://doi.org/10.1029/2002PA000768, 2003.

Bartlein, P. J., Anderson, K. H., Anderson, P. M., Edwards, M. E., Mock, C. J., Thompson, R. S., Webb, R. S., Webb, T. and Whitlock, C.: Paleoclimate simulations for North America over the past 21,000 years: Features of the simulated climate and comparisons with paleoenvironmental data, Quat. Sci. Rev., 17(6-7), 549–585, doi:10.1016/S0277-3791(98)00012-2, 1998.

Berger A. and Loutre M. F.: Insolation values for the climate of the last 10 million years. Quat. Sci. Rev., 10, pp. 297-317, 1991

Berman, D., Alfimov, A. and Kuzmina, S.: Invertebrates of the relict steppe ecosystems of Beringia, and the reconstruction of Pleistocene landscapes, Quat. Sci. Rev., 30(17-18), 2200–2219, doi:10.1016/j.quascirev.2010.09.016, 2011.

Bigelow, N. H. and Edwards, M. E.: A 14000 yr paleoenvironmental record from Windmill Lake, central Alaska: evidence for high-frequency climatic and vegetation fluctuations, Quat. Sci. Rev., 20, 203–215, 2001.

Bigelow, N.H. and Powers, W.M.R.: Climate, vegetation and archaeology 14 000-9000 cal yr BP in central Alaska. Arctic Anthropol. 38, 171-195, 2001.

Braconnot, P., Harrison, S. P., Kageyama, M., Bartlein, P. J., Masson-delmotte, V., Abe-ouchi, A., … Zhao, Y. . Evaluation of climate models using palaeoclimatic data. Nature Climate Change, 2(6), 417–424. http://doi.org/10.1038/nclimate1456, 2012.

Brooks, S. J., Diekmann, B., Jones, V. J. and Hammarlund, D.: Holocene environmental change in Kamchatka: A synopsis, Glob. Planet. Change, 134, 166–174, doi:10.1016/j.gloplacha.2015.09.004, 2015.

Brovkin, V., Raddatz, T. Reick, C., Claussen, M. and Gayler, V.: Global biogeophysical interactions between forest and climate, Geophys. Res. Lett. 36, L07405, doi:10.1029/2009GL037543, 2009.Brubaker, L. B., Anderson, P. M. and Hu, F. S.: Vegetation ecotone dynamics in southwest Alaska during the late Quaternary, Quat. Sci. Rev. 20, 175–188, 2001.

Caissie, B. E., Brigham-Grette, J., Lawrence, K. T., Herbert, T. D. and Cook, M. S.: Last Glacial Maximum to Holocene sea surface conditions at Umnak Plateau, Bering Sea, as inferred from diatom, alkenone, and stable isotope records, Paleoceanography, 25(1), PA1206, doi:10.1029/2008PA001671, 2010.

Chikamoto, M. O., Menviel, L., Abe-Ouchi, A., Ohgaito, R., Timmermann, A., Okazaki, Y., Harada, N., Oka, A. and Mouchet, A.: Variability in North Pacific intermediate and deep water ventilation during Heinrich events in two coupled climate models, Deep Sea Res. Part II Top. Stud. Oceanogr., 61-64, 114–126, doi:10.1016/j.dsr2.2011.12.002, 2012.

De Jonge, C., Stadnitskaia, A., Hopmans, E. C., Cherkashov, G., Fedotov, A. and Sinninghe Damsté, J. S.: In situ produced branched glycerol dialkyl glycerol tetraethers in suspended particulate matter from the Yenisei River, Eastern Siberia, Geochim. Cosmochim. Acta, 125, 476–491, doi:10.1016/j.gapprox.2013.10.031, 2014.

de Vernal, A. and Pedersen, T. F.: Micropaleontology and palynology of core PAR87A-10: A 23,000 year record of paleoenvironmental changes in the Gulf of Alaska, northeast North Pacific, Paleoceanography, 12(6), 821, doi:10.1029/97PA02167, 1997.

Dirksen, V., Dirksen, O. and Diekmann, B.: Holocene vegetation dynamics and climate change in Kamchatka Peninsula, Russian Far East, Rev. Palaeobot. Palynol., 190, 48–65, doi:10.1016/j.revpalbo.2012.11.010, 2013.

Dirksen, V., Dirksen, O., van den Bogaard, C. and Diekmann, B.: Holocene pollen record from Lake Sokoch, interior Kamchatka (Russia), and its paleobotanical and paleoclimatic interpretation, Glob. Planet. Change, 134, 129–141, doi:10.1016/j.gloplacha.2015.07.010, 2015.

Dong, B. and Valdes, P. J.: Simulations of the Last Glacial Maximum climates using a general circulation model: prescribed versus computed sea surface temperatures, Clim. Dyn., 14, 571– 591, 1998.

Dong, L., Li, Q., Li, L. and Zhang, C. L.: Glacial – interglacial contrast in MBT/CBT proxies in the South China Sea: Implications for marine production of branched GDGTs and continental teleconnection, Org. Geochem., 79, 74–82, doi:10.1016/j.orggeochem.2014.12.008, 2015.

Dullo, W. C., Baranov, B. and van den Bogaard, C.: FS Sonne Fahrtbericht/Cruise Report SO201–2. IFM-GEOMAR, Report 35, Kiel, IFM262 GEOMAR, 2009.

Elias, S., and Crocker, B.: The Bering Land Bridge: a moisture barrier to the dispersal of steppe–tundra biota? Quat. Sci. Rev., 27, 2473–2483. http://doi.org/10.1016/j.quascirev.2008.09.011, 2008.

Elias, S. A., Short, S. K. and Birks, H. H.: Late Wisconsin environments of the Bering Land Bridge, Palaeogeogr. Palaeoclimatol. Palaeoecol., 136(1-4), 293–308, doi:10.1016/S0031-0182(97)00038-2, 1997.

Elias, S. A., Short, S. K., Nelson, C. H. and Birks, H. H.: Life and times of the Bering land bridge, Nature, 382(6586), 60–63, doi:10.1038/382060a0, 1996.

Elias, S. A.: Mutual climatic range reconstructions of seasonal temperatures based on Late Pleistocene fossil beetle assemblages in Eastern Beringia, Quat. Sci. Rev., 20, 77–91, doi:10.1016/S0277-3791(00)00130-X, 2001.

Fritz, M., Herzschuh, U., Wetterich, S., Lantuit, H., De Pascale, G. P., Pollard, W. H., and Schirrmeister, L.: Late glacial and Holocene sedimentation, vegetation, and climate history from easternmost Beringia (northern Yukon Territory, Canada). Quat. Res., 78(3), 549–560. http://doi.org/10.1016/j.yqres.2012.07.007, 2012.

Glebova, S., Ustinova, E. and Sorokin, Y.: Long-term changes of atmospheric centers and climate regime of the Okhotsk Sea in the last three decades. PICES Sci. Rep. 36, 3–9, 2009.

Gong, X., Knorr, G., Lohmann, G. and Zhang, X.: Dependence of abrupt Atlantic meridional ocean circulation changes on climate background states. Geophys. Res. Lett. 40 (14), 3698–3704, doi:10.1002/grl.50701, 2013.

Guthrie, R. D.: Origin and causes of the mammoth steppe: a story of cloud cover, woolly mammal tooth pits, buckles, and inside-out Beringia, Quat. Sci. Rev., 20, 549–574, 2001.

Hammarlund, D., Klimaschewski, A., St. Amour, N. A., Andrén, E., Self, A. E., Solovieva, N., Andreev, A. A., Barnekow, L. and Edwards, T. W. D.: Late Holocene expansion of Siberian dwarf pine (Pinus pumila) in

Kamchatka in response to increased snow cover as inferred from lacustrine oxygen-isotope records, Glob. Planet. Change, 134, 91–100, doi:10.1016/j.gloplacha.2015.04.004, 2015.

Harada, N., Ahagon, N., Uchida, M. and Murayama, M.: Northward and southward migrations of frontal zones during the past 40 kyr in the Kuroshio – Oyashio transition area. Geochem. Geophys. Geosyst. 5, Q09004, 2004.

Harada, N., Sato, M., Seki, O., Timmermann, A., Moossen, H., Bendle, J., Nakamura, Y., Kimoto, K., Okazaki, Y., Nagashima, K., Gorbarenko, S. A., Ijiri, A., Nakatsuka, T., Menviel, L., Chikamoto, M. O., Abe-Ouchi, A. and Schouten, S.: Sea surface temperature changes in the Okhotsk Sea and adjacent North Pacific during the last glacial maximum and deglaciation, Deep Sea Res. Part II Top. Stud. Oceanogr., 61-64, 93–105, doi:10.1016/j.dsr2.2011.12.007, 2012.

Hoff, U., Dirksen, O., Dirksen, V., Kuhn, G., Meyer, H. and Diekmann, B.: Holocene freshwater diatoms: palaeoenvironmental implications from south Kamchatka, Russia, Boreas, 43(1), 22–41, doi:10.1111/bor.12019, 2014.

Hoff, U., Biskaborn, B. K., Dirksen, V. G., Dirksen, O., Kuhn, G., Meyer, H., Nazarova, L., Roth, A. and Diekmann, B.: Holocene environment of Central Kamchatka, Russia: Implications from a multi-proxy record of Two-Yurts Lake, Glob. Planet. Change, 134, 101–117, doi:10.1016/j.gloplacha.2015.07.011, 2015.

Hopkins, D. M., Matthews Jr., J. V., Schweger, C. E. and Young, S. B. (Eds.): Paleoecology of Beringia. Academic Press, New York, 1982.

Hopmans, E. C., Schouten, S., Pancost, R. D., Van Der Meer, M. T. J., & Sinninghe Damsté, J. S.. Analysis of intact tetraether lipids in archaeal cell material and sediments by high performance liquid chromatography/atmospheric pressure chemical ionization mass spectrometry. Rapid Commun. Mass Spectrom: RCM, 14(7), 585–9, 2000.

Hopmans, E. C., Weijers, J. W. ., Schefuß, E., Herfort, L., Sinninghe Damsté, J. S. and Schouten, S.: A novel proxy for terrestrial organic matter in sediments based on branched and isoprenoid tetraether lipids, Earth Planet. Sci. Lett., 224(1-2), 107–116, doi:10.1016/j.epsl.2004.05.012, 2004.

Climate data from Klyuchi climate station. http://en.climate-data.org/location/284590/, 2015

Ivanov, A.: The Far East. In: The Physical Geography of Northern Eurasia, Shahgedanova M. (ed.). Oxford University Press: Oxford, 422-447, 2002.

Jungclaus, J. H., Keenlyside, N., Botzet, M., Haak, H., Luo, J.-J., Latif, M., Marotzke, J., Mikolajewic, M. and Roeckner, E.: Ocean circulation and tropical variability in the coupled model ECHAM5/MPI-OM, J. Climate, 19, 3952–3972, 2006.

Jones, V. and Solomina, O.: The Geography of Kamchatka, Glob. Planet. Change, 134, 3–9, doi:10.1016/j.gloplacha.2015.06.003, 2015.

Kageyama, M., Laîné, a., Abe-Ouchi, a., Braconnot, P., Cortijo, E., Crucifix, M., de Vernal, a., Guiot, J., Hewitt, C. D., Kitoh, a., Kucera, M., Marti, O., Ohgaito, R., Otto-Bliesner, B., Peltier, W. R., Rosell-Melé, a., Vettoretti, G., Weber, S. L. and Yu, Y.: Last Glacial Maximum temperatures over the North Atlantic, Europe and western Siberia: a comparison between PMIP models, MARGO sea-surface temperatures and pollen-based reconstructions, Quat. Sci. Rev., 25(17-18), 2082–2102, doi:10.1016/j.quascirev.2006.02.010, 2006.

Kiefer, T. and Kienast, M.: Patterns of deglacial warming in the Pacific Ocean: a review with emphasis on the time interval of Heinrich event 1, Quat. Sci. Rev., 24(7-9), 1063–1081, doi:10.1016/j.quascirev.2004.02.021, 2005.

Kienast, F.: Die Rekonstruktion der spätquartären Vegetations- und Klimageschichte der Laptewsee-Region auf der Basis botanischer Großrestuntersuchungen. Ph.D. Dissertation, Potsdam University, 116pp, 2002.

Kienast, F., Schirrmeister, L., Siegert, C. and Tarasov, P.: Palaeobotanical evidence for warm summers in the East Siberian Arctic during the last cold stage, Quat. Res., 63(3), 283–300, doi:10.1016/j.yqres.2005.01.003, 2005.

Kim, S. J., Crowley, T. J., Erickson, D. J., Govindasamy, B., Duffy, P. B. and Lee, B. Y.: High-resolution climate simulation of the last glacial maximum, Clim. Dyn., 31(1), 1–16, doi:10.1007/s00382-007-0332-z, 2008.

Kiselev, S. V.: Beetles in North-East Siberia during the Late Cenozoic. Nauka Press, Moscow, 1981 (in Russian).

Klimaschewski, A., Barnekow, L., Bennett, K. D., Andreev, A. A., Andrén, E., Bobrov, A. A. and Hammarlund, D.: Holocene environmental changes in southern Kamchatka, Far Eastern Russia, inferred from a pollen and

testate amoebae peat succession record, Glob. Planet. Change, 134, 142–154, doi:10.1016/j.gloplacha.2015.09.010, 2015.

Knorr, G. and Lohmann, G.: Climate warming during Antarctic ice sheet expansion at the Middle Miocene transition, Nature Geosci. 7, 376–381, 2014.

Kokorowski, H. D., Anderson, P. M., Mock, C. J. and Lozhkin, A. V.: A re-evaluation and spatial analysis of evidence for a Younger Dryas climatic reversal in Beringia, Quat. Sci. Rev., 27, 1710–1722, doi:10.1016/j.quascirev.2008.06.010, 2008a.

Kokorowski, A. H. D., Anderson, P. M., Sletten, R. S., Lozhkin, A. V. and Brown, T. A.: Late Glacial and Early Holocene Climatic Changes Based on a Multiproxy Lacustrine Sediment Record from Northeast Siberia, Arctic, Antarct. Alp. Res., 40(3), 497–505, doi:10.1657/1523-0430(07-036), 2008b.

Kondratyuk, V. I.: Climate of Kamchatka. Hydrometeoizdat, Moscow, 1974 (In Russian).

Kuehn, H., Lembke-Jene, L., Gersonde, R., Esper, O., Lamy, F., Arz, H., Kuhn, G. and Tiedemann, R.: Laminated sediments in the Bering Sea reveal atmospheric teleconnections to Greenland climate on millennial to decadal timescales during the last deglaciation, Clim. Past, 10(6), 2215–2236, doi:10.5194/cp-10-2215-2014, 2014.

Kurek, J., Cwynar, L. C., Ager, T. A., Abbott, M. B. and Edwards, M. E.: Late Quaternary paleoclimate of western Alaska inferred from fossil chironomids and its relation to vegetation histories, Quat. Sci. Rev., 28(9-10), 799–811, doi:10.1016/j.quascirev.2008.12.001, 2009.

Kutzbach, J., Gallimore, R., Harrison, S., Behling, P., Selin, R. and Laarif, F.: Climate and Biome simulations for the past 21,000 years, Quat. Sci. Rev., 17(6-7), 473–506, 1998.

Kutzbach, J. E. and Wright, E.: Simulation of the climate of 18 000 years BP: results for the North American / North Atlantic/ European sector and comparison with the geological record of North America, Quart. Sci. Rev., 4, 147–185, 1985.

Lohmann, G., Pfeiffer, M., Laepple, T., Leduc, G. and Kim, J.-H.: A model-data comparison of the Holocene global sea surface temperature evolution, Clim. Past, 9, 1807-1839, 2013

Lozhkin, A. V. and Anderson, P. M.: A late Quaternary pollen record from Elikchan 4 Lake, northeast Siberia, Geol. Pac. Ocean, 12, 609–616, 1996.

Lozhkin, A. V. Anderson, P. M. Ravako, L. G. Hopkins, D. M. Brubaker, L. B., Colinvaux, P. A. Miller, M. C.: Late Quaternary Lacustrine Pollen Records from Southwestern Beringia, Quat. Res., 39, 314–324, 1993.

Lozhkin, A. V., Anderson, P. M., Vartanyan, S. L., Brown, T. A., Belaya, B. V. and Kotov, A. N.: Late Quaternary palaeoenvironments and modern pollen data from Wrangel Island (Northern Chukotka), Quat. Sci. Rev., 20(1-3), 217–233, doi:10.1016/S0277-3791(00)00121-9, 2001.

Lozhkin, A. V., Anderson, P. M., Matrosova, T. V. and Minyuk, P. S.: The pollen record from El'gygytgyn Lake: Implications for vegetation and climate histories of northern Chukotka since the late middle Pleistocene, J. Paleolimnol., 37(1), 135–153, doi:10.1007/s10933-006-9018-5, 2007.

Lund, D. C., Mix, A. C. and Southon, J.: Increased ventilation age of the deep northeast Pacific Ocean during the last deglaciation, Nat. Geosci., 4(11), 771–774, doi:10.1038/ngeo1272, 2011.

Maier, E., Méheust, M., Abelmann, A., Gersonde, R., Chapligin, B., Ren, J., Stein, R., Meyer, H. and Tiedemann, R.: Deglacial subarctic Pacific surface water hydrography and nutrient dynamics and links to North Atlantic climate variability and atmospheric CO_2, Paleoceanography, 30(7), 949–968, doi:10.1002/2014PA002763, 2015.

Manabe, S. and Stouffer, R. J.: Two stable equilibria of a coupled ocean-atmosphere model. J. Climate, 1, 841-861, 1988.

Marsland, S. J., Haak, H., Jungclaus, J. H., Latif, M. and Röske, F.: The Max-Planck-Institute global ocean/sea ice model with orthogonal curvilinear coordinates. Ocean Modell. 5, 91–127, doi:10.1016/S1463-5003(02)00015-X, 2003.

Mason, O.K., Bowers, P.M., and Hopkins, D.M.: The early Holocene Milankovitch thermal maximum and humans: Adverse conditions for the Denali complex of eastern Beringia. Quat. Sci. Rev. 20, 525–548, 2001

Matthews Jr., J.V. and Telka, A.: Insect fossils from the Yukon. In: Danks, H.V., Downes, J.A. (Eds.), Insects of the Yukon. Ottawa, Biological Survey of Canada (Terrestrial Arthropods), pp. 911-962, 1997.

Max, L., Riethdorf, J.-R., Tiedemann, R., Smirnova, M., Lembke-Jene, L., Fahl, K., Nürnberg, D., Matul, A. and Mollenhauer, G.: Sea surface temperature variability and sea-ice extent in the subarctic northwest Pacific during the past 15,000 years, Paleoceanography, 27(3), PA3213, doi:10.1029/2012PA002292, 2012.

Meyer, H., Dereviagin, A., Siegert, C., Schirrmeister, L. and Hubberten, H.-W.: Palaeoclimate reconstruction on Big Lyakhovsky Island, north Siberia - Hydrogen and oxygen isotopes in ice wedges, Permafr. Periglac. Process., 13(2), 91–105, doi:10.1002/ppp.416, 2002.

Meyer, V. D., Max, L., Hefter, J., Tiedemann, R. and Mollenhauer, G.: Glacial-to-Holocene evolution of sea surface temperature and surface circulation in the subarctic northwest Pacific and the Western Bering Sea, Paleoceanography, 31, 916-927, doi:10.1002/2015PA002877, 2016.

Meyer, H., Schirrmeister, L., Yoshikawa, K., Opel, T., Wetterich, S., Hubberten, H. W. and Brown, J.: Permafrost evidence for severe winter cooling during the Younger Dryas in northern Alaska, Geophys. Res. Lett., 37(3), 1–5, doi:10.1029/2009GL041013, 2010.

Mikolajewicz, U., Crowley, T. J., Schiller, A. and Voss, R.: Modelling teleconnections between the North Atlantic and North Pacific during the Younger Dryas, Nature, 387, 384–387, 1997.

Mix, A. C., Bard, E. and Schneider, R.: Environmental processes of the ice age: land, ocean, glaciers (ELIPOG). Quat. Sci. Rev., 20, 627-657, 2001.

Mock, C. J., Mock, C. J., Bartlein, P. J., Bartlein, P. J., Anderson, P. a and Anderson, P. A.: Atmospheric circulation patterns and spatial climatic variations, Beringia, Int. J. Climatol., 10, 1085–1104, 1998.

Monnin, E., Indermühle, A., Dällenbach, A., Flückiger, J., Stauffer, B., Stocker, T. F., Raynaud, D. and Barnola, J. M.: Atmospheric CO_2 concentrations over the last glacial termination, Science, 291(5501), 112–114, doi:10.1126/science.291.5501.112, 2001.

Nazarova, L., de Hoog, V., Hoff, U., Dirksen, O. and Diekmann, B.: Late Holocene climate and environmental changes in Kamchatka inferred from the subfossil chironomid record, Quat. Sci. Rev., 67, 81–92, doi:10.1016/j.quascirev.2013.01.018, 2013.

Nolan, M., Liston, G., Prokein, P., Brigham-Grette, J., Sharpton, V. L. and Huntzinger, R.: Analysis of lake ice dynamics and morphology on Lake El'gygytgyn, NE Siberia, Siberia, using synthetic aperture radar (SAR) and Landsat, J. Geophys. Res., 108, 1–12, 2003.

North Greenland Ice Core Project members: High-resolution record of northern hemisphere climate extending into the last interglacial period, Nature, 431, 147–151, doi:10.1038/nature02805, 2004.

Nowaczyk, N. R., Minyuk, P., Melles, M., Brigham-Grette, J., Glushkova, O., Nolan, M., Lozhkin, A. V., Stetsenko, T. V., Anderson, P. M. and Forman, S. L.: Magneto-stratigraphic results from impact crater Lake El'gygytgyn, northeast Siberia: a 300 kyr long high-resolution terrestrial palaeoclimatic record from the Arctic, Geophys. J. Int., 150, 109–126, 2002.

Parrenin, F., Masson-Delmotte, V., Köhler, P., Raynaud, D., Paillard, D., Schwander, J., … Jouzel, J.: Synchronous change of atmospheric CO_2 and Antarctic temperature during the last deglacial warming. Science (New York, N.Y.), 339(6123), 1060–3. http://doi.org/10.1126/science.1226368, 2013.

Peterse, F., Kim, J.-H., Schouten, S., Kristensen, D. K., Koç, N. and Sinninghe Damsté, J. S.: Constraints on the application of the MBT/CBT palaeothermometer at high latitude environments (Svalbard, Norway), Org. Geochem., 40(6), 692–699, doi:10.1016/j.orggeochem.2009.03.004, 2009.

Peterse, F., van der Meer, J., Schouten, S., Weijers, J. W. H., Fierer, N., Jackson, R. B., Kim, J.-H. and Sinninghe Damsté, J. S.: Revised calibration of the MBT–CBT paleotemperature proxy based on branched tetraether membrane lipids in surface soils, Geochim. Cosmochim. Acta, 96, 215–229, doi:10.1016/j.gapprox.2012.08.011, 2012.

Peterse, F., Vonk, J., Holmes, M., Giosan, L., Zimov, N. and Eglinton, T. I.: Branched glycerol dialkyl glycerol tetraethers in Arctic lake sediments: Sources and implications for paleothermometry at high latitudes, J. Geophys. Res. Biogeosciences, 119, 1738–1754, doi:10.1002/2014JG002639., 2014.

Pisaric, M. F. J., MacDonald, G. M., Velichko, A. A. and Cwynar, L. C.: The late-glacial and post-glacial vegetation history of the northwestern limits of Beringia based on pollen, stomates, and tree stump evidence, Quat. Sci. Rev., 20, 235–245, 2001.

Pitul'ko, V. V., Pavlova, E. Y., Kuz'mina, S. A., Nikol'skii, P. A., Basilyan, A. E., Tumskoi, V. E. and Anisimov, M. A.: Natural-climatic changes in the Yana-Indigirka lowland during the terminal Kargino time and habitat of late Paleolithic man in northern part of East Siberia, Dokl. Earth Sci., 417(1), 1256–1260, doi:10.1134/S1028334X07080284, 2007.

Praetorius, S. K. and Mix, A. C.: Synchronization of North Pacific and Greenland climates preceded abrupt deglacial warming, Science, 345(6195), 444–8, doi:10.1126/science.1252000, 2014.

Praetorius, S. K., Mix, A. C., Walczak, M. H., Wolhowe, M. D., Addison, J. A., & Prahl, F. G.: North Pacific deglacial hypoxic events linked to abrupt ocean warming. Nature, 527(7578), 362–366. http://doi.org/10.1038/nature15753, 2015.

Raddatz, T. J., Reick, C. H., Knorr, W., Kattge, J., Roeckner, E., Schnur, R., Schnitzler, K.-G., Wetzel, P., and Jungclaus, J.: Will the tropical land biosphere dominate the climate–carbon cycle feedback during the twenty-first century?, Clim. Dynam., 29, 565–574, 2007.

Reimer, P.J., Baillie, M.G., Bard, E., Bayliss, A., Beck, J.W., Blackwell, P.G., Bronk Ramsey, C., Buck, C.E., Burr, G.S., Edwards, R.L., Friedrich, M., Grootes, P.M., Guilderson, T.P., Hajdas, I., Heaton, T.J., Hogg, A.G., Hughen, K.A., Kaiser, K.F., Kromer, B., McCormac, F.G., Manning, S.W., Reimer, R.W., Richards, D.A., Southon, J.R., Talamo, S., Turney, C.S.M., van der Plicht, J. and Weyhenmeyer, C.E.: Intcal09 and marine09 radiocarbon age calibration curves, 0–50,000 years cal BP. Radiocarbon 51, 1111–1150, 2009.

Roeckner, E., Brokopf, R., Esch, M., Giorgetta, M., Hagemann, S. and Kornbueh, L.: Sensitivity of simulated climate to horizontal and vertical resolution in the ECHAM5 Atmosphere Model, J. Climate, 19, 3771–3791, doi:10.1175/JCLI3824.1, 2006.

Rueda, G., Rosell-Melé, A., Escala, M., Gyllencreutz, R. and Backman, J.: Comparison of instrumental and GDGT-based estimates of sea surface and air temperatures from the Skagerrak, Org. Geochem., 40(2), 287–291, doi:10.1016/j.orggeochem.2008.10.012, 2009.

Sarnthein, M., Balmer, S., Grootes, P. M., and Mudelsee, M.: Planktic and Benthic ^{14}C Reservoir Ages for Three Ocean Basins, Calibrated by a Suite of ^{14}C Plateaus in the Glacial-to-Deglacial Suigetsu Atmospheric ^{14}C record. Radiocarbon, Vol 57, 1, 2015, p 129–151, 2015.

Savoskul, O. S.: Holocene glacier advances in the headwaters of Sredniaya Avacha, Kamchatka, Russia. Qual. Res. 52, 14–26, 1999.

Schouten, S., Huguet, C., Hopmans, E. C., and Sinninghe Damsté, J. S.: Improved analytical methodology of the TEX_{86} paleothermometry by high performance liquid chromatography/atmospheric pressure chemical ionization-mass spectrometry, Anal. Chem., 79, 2940–2944, 2007.

Seki, O., Bendle, J. a., Harada, N., Kobayashi, M., Sawada, K., Moossen, H., Inglis, G. N., Nagao, S. and Sakamoto, T.: Assessment and calibration of TEX_{86} paleothermometry in the Sea of Okhotsk and sub-polar North Pacific region: Implications for paleoceanography, Prog. Oceanogr., 126, 254–266, doi:10.1016/j.pocean.2014.04.013, 2014.

Seki, O., Kawamura, K., Ikehara, M., Nakatsuka, T. and Oba, T.: Variation of alkenone sea surface temperature in the Sea of Okhotsk over the last 85 kyrs, Org. Geochem., 35(3), 347–354, doi:10.1016/j.orggeochem.2003.10.011, 2004.

Seki, O., Sakamoto, T., Sakai, S., Schouten, S., Hopmans, E. C., Sinninghe Damste, J. S. and Pancost, R. D.: Large changes in seasonal sea ice distribution and productivity in the Sea of Okhotsk during the deglaciations, Geochemistry, Geophys. Geosystems, 10(10), Q10007, doi:10.1029/2009GC002613, 2009.

Self, A. E., Klimaschewski, A., Solovieva, N., Jones, V. J., Andrén, E., Andreev, A. A., Hammarlund, D. and Brooks, S. J.: The relative influences of climate and volcanic activity on Holocene lake development inferred from a mountain lake in central Kamchatka, Glob. Planet. Change, 134, 67–81, doi:10.1016/j.gloplacha.2015.06.012, 2015.

Shakun, J. D., Clark, P. U., He, F., Marcott, S. A., Mix, A. C., Liu, Z., Otto-Bliesner, B., Schmittner, A. and Bard, E.: Global warming preceded by increasing carbon dioxide concentrations during the last deglaciation, Nature, 484(7392), 49–54, doi:10.1038/nature10915, 2012.

Shanahan, T. M., Hughen, K. A. and Van Mooy, B. A. S.: Temperature sensitivity of branched and isoprenoid GDGTs in Arctic lakes, Org. Geochem., 64, 119–128, doi:10.1016/j.orggeochem.2013.09.010, 2013.

Sher, A. V., Kuzmina, S. A., Kuznetsova, T. V. and Sulerzhitsky, L. D.: New insights into the Weichselian environment and climate of the East Siberian Arctic, derived from fossil insects, plants, and mammals, Quat. Sci. Rev., 24(5-6), 533–569, doi:10.1016/j.quascirev.2004.09.007, 2005.

Smirnova, M. A., Kazarina, G. K., Matul, A. G. and Max, L.: Diatom Evidence for Paleoclimate Changes in the Northwestern Pacific during the Last 20000 Years, Mar. Geol., 55(3), 425–431, doi:10.1134/S0001437015030157, 2015.

Solovieva, N., Klimaschewski, A., Self, A. E., Jones, V. J., Andrén, E., Andreev, A. A., Hammarlund., D., Lepskaya, E. V. and Nazarova, L.: The Holocene environmental history of a small coastal lake on the north-eastern Kamchatka Peninsula, Glob. Planet. Change, 134, 55–66, doi:10.1016/j.gloplacha.2015.06.010, 2015.

Stabeno, P. J., and Reed, R. K.: Circulation in the Bering Sea basin by satellite tracked drifters. J. Phys. Oceanogr., 24(4), 848-854, 1994.

Stärz, M., G. Lohmann, and G. Knorr. The effect of a dynamic soil scheme on the climate of the mid-Holocene and the Last Glacial Maximum. Clim. Past 12, 151-170. doi:10.5194/cp-12-151-2016, 2016.

Stepanek, C., and Lohmann, G.: Modelling mid-Pliocene climate with COSMOS, Geosci. Model Dev., 5, 1221-1243, 2012.

Stuiver, M., and Reimer, P.J.: Extended C-14 Data-Base and Revised Calib 3.0 C-14 Age Calibration Program, Radiocarbon, 35(1), 215–230, 1993.

Ternois, Y. T., Awamura, K. K., Hkouchi, N. O. and Eigwin, L. K.: Alkenone sea surface temperature in the Okhotsk Sea for the last 15 kyr, Geochem. J., 34, 283–293, 2000.

Vettoretti, G., Peltier, W. R., and McFarlane, N. A.: Global water balance and atmospheric water vapor transport at last glacial maximum: climate simulations with the Canadian Climate Center for Modelling and Analysis atmospheric general circulation model, Can. J. Earth Sci., 37, 695–723, 2000.

Vellinga, M. and R. A. Wood, R. A.: Global climate impacts of a collapse of the Atlantic thermohaline circulation, Clim. Chang., 54(3), 251-267, doi:10,1023/A:1016168827653, 2002.

Waelbroeck, C., Paul, A., Kucera, M., Rosell-Melé, A., Weinelt, M., Schneider, R., Mix, a. C., Abelmann, A., Armand, L., Bard, E., Barker, S., Barrows, T. T., Benway, H., Cacho, I., Chen, M.-T., Cortijo, E., Crosta, X., de Vernal, A., Dokken, T., Duprat, J., Elderfield, H., Eynaud, F., Gersonde, R., Hayes, A., Henry, M., Hillaire-Marcel, C., Huang, C.-C., Jansen, E., Juggins, S., Kallel, N., Kiefer, T., Kienast, M., Labeyrie, L., Leclaire, H., Londeix, L., Mangin, S., Matthiessen, J., Marret, F., Meland, M., Morey, A. E., Mulitza, S., Pflaumann, U., Pisias, N. G., Radi, T., Rochon, A., Rohling, E. J., Sbaffi, L., Schäfer-Neth, C., Solignac, S., Spero, H., Tachikawa, K. and Turon, J.-L.: Constraints on the magnitude and patterns of ocean cooling at the Last Glacial Maximum, Nat. Geosci., 2, 127–132, doi:10.1038/ngeo411, 2009.

Weber, M. E., Clark, P. U., Kuhn, G., Timmermann, A., Sprenk, D., Gladstone, R., Zhang, X., Lohmann, G., Menviel, L., Chikamoto, M. O., Friedrich, T. and Ohlwein, C.: Millennial-scale variability in Antarctic ice-sheet discharge during the last deglaciation, Nature 510, 134–138, doi:10.1038/nature13397, 2014

Wei, W., Lohmann, G. and Dima, M.: Distinct modes of internal variability in the Global Meridional Overturning Circulation associated to the Southern Hemisphere westerly winds, J. Phys. Oceanogr., 42, 785–801. doi:10.1175/JPO-D-11-038.1, 2012

Wei, W., and Lohmann, G.: Simulated Atlantic Multidecadal Oscillation during the Holocene, J. Climate, 25, 6989–7002. doi:10.1175/JCLI-D-11-00667.1, 2012

Weijers, J. W. H., Schouten, S., Hopmans, E. C., Geenevasen, J. A. J., David, O. R. P., Coleman, J. M., Pancost, R. D. and Sinninghe Damsté, J. S.: Membrane lipids of mesophilic anaerobic bacteria thriving in peats have typical archaeal traits, Environ. Microbiol. 8, 648–657, 2006a

Weijers, J. W. H., Schouten, S., Spaargaren, O. C. and Sinninghe Damsté, J. S.: Occurrence and distribution of tetraether membrane lipids in soils: Implications for the use of the TEX_{86} proxy and the BIT index, Org. Geochem., 37(12), 1680–1693, doi:10.1016/j.orggeochem.2006.07.018, 2006b.

Weijers, J. W. H., Schouten, S., van den Donker, J. C., Hopmans, E. C. and Sinninghe Damsté, J. S.: Environmental controls on bacterial tetraether membrane lipid distribution in soils, Geochim. Cosmochim. Acta, 71(3), 703–713, doi:10.1016/j.gapprox.2006.10.003, 2007.

Yanase, W. and Abe-Ouchi, A.: The LGM surface climate and atmospheric circulation over East Asia and the North Pacific in the PMIP2 coupled model simulations, Clim. Past, 3(3), 439–451, doi:10.5194/cp-3-439-2007.

Yanase, W. and Abe-Ouchi, A.: A numerical study on the atmospheric circulation over the midlatitude North Pacific during the last glacial maximum, J. Clim., 23(1), 135–151, doi:10.1175/2009JCLI3148.1, 2010.

Zell, C., Kim, J.-H., Hollander, D., Lorenzoni, L., Baker, P., Silva, C. G., Nittrouer, C. and Sinninghe Damsté, J. S.: Sources and distributions of branched and isoprenoid tetraether lipids on the Amazon shelf and fan: Implications for the use of GDGT-based proxies in marine sediments, Geochim. Cosmochim. Acta, 139, 293–312, doi:10.1016/j.gapprox.2014.04.038, 2014.

Zell, C., Kim, J.-H., Moreira-Turcq, P., Abril, G., Hopmans, E. C., Bonnet, M.-P., Lima Sobrinho, R. and Sinninghe Damsté, J. S.: Disentangling the origins of branched tetraether lipids and crenarchaeol in the lower Amazon River: Implications for GDGT-based proxies, Limnol. Oceanogr., 58(1), 343–353, doi:10.4319/lo.2013.58.1.0343, 2013.

Zhang, X., Lohmann, G., Knorr, G. and Purcell, C.: Abrupt glacial climate shifts controlled by ice sheet changes. Nature 512, 290–294, DOI: 10.1038/nature13592, 2014.

Zhang, X., Lohmann, G., Knorr, G. and Xu, X. Different ocean states and transient characteristics in Last Glacial Maximum simulations and implications for deglaciation. Clim. Past 9, 2319-2333, doi:10.5194/cp-9-2319-2013, 2013.

Zhu, C., Weijers, J. W. H., Wagner, T., Pan, J.-M., Chen, J.-F. and Pancost, R. D.: Sources and distributions of tetraether lipids in surface sediments across a large river-dominated continental margin, Org. Geochem., 42(4), 376–386, doi:10.1016/j.orggeochem.2011.02.

Figure captions

Figure 1. (a) Overview of Beringia and the N Pacific. Site SO201-2-12KL is marked by a red star. Circles represent sites mentioned in the text. Black arrows indicate the surface circulation patterns of the N Pacific (e.g. Stabeno and Reed, 1994). BLB = Bering Land Bridge, KR = Kankaren Range, R = River, EKC = East Kamchatka Current. P = Peninsula. L= Lake (b) Map of the Kamchatka Peninsula and its major orographic units. CKD = Central Kamchatka Depression.

Figure 2. a) Concentrations of ΣbrGDGT of core 12KL. b) CBT/MBT' derived MAT_{ifs} from Kamchatka (this study). Black pins represent the age control points from core 12KL (based on radiocarbon dating of planktonic

foraminifera, Max et al., 2012). c) BIT-index values of core 12KL (Meyer et al., 2016). d) Titanium/Calcium ratios (Ti/Ca, XRF-scan core 12KL, Max et al., 2012). e) Mean July insolation at 65°N (Berger and Loutre, 1991). f) Atmospheric CO_2 concentration (EPICA dome C, Monnin et al., 2001; Parrenin et al., 2013). g) SST development in the marginal NW Pacific (site 12KL, Meyer et al., submitted). h) SST evolution in the western Bering Sea (site 114KL, Meyer et al., 2016). i) NGRIP-$\delta^{18}O$ (NGRIP, 2004) represents climate change in the N Atlantic. Grey-shaded bars mark the HS1 and YD stadials.

Figure 3. Fractional abundances of all nine brGDGT in core 12KL, given in percentage relative to the amount of ΣbrGDGTs.

Figure 4. Comparison of proxy- and model-based inferences regarding glacial anomalies in temperature and atmospheric circulation over the N Pacific and Beringia relative to present. (A) COSMOS-simulation for the JJA SLP-anomaly over Beringia and the N Pacific during the LGM (21 ka) relative to PI. Arrows represent the wind anomaly. Note that the model predicts a northerly anomaly over Kamchatka. (B) COSMOS-simulation for the SAT and wind-anomalies during JJA. (C) Compilation of proxy based anomalies of summer air temperature in Beringia and of summer/autumn SST reconstructions in the N Pacific for the LGM. Sites and corresponding references are given in the appendix, Table A1. Doted arrows sketch the general summer anticyclone over the N Pacific, the NPH. Based on MAT_{ifs}, the NPH and associated southerly winds over the subarctic NW Pacific were stronger than at present (represented by solid arrow).

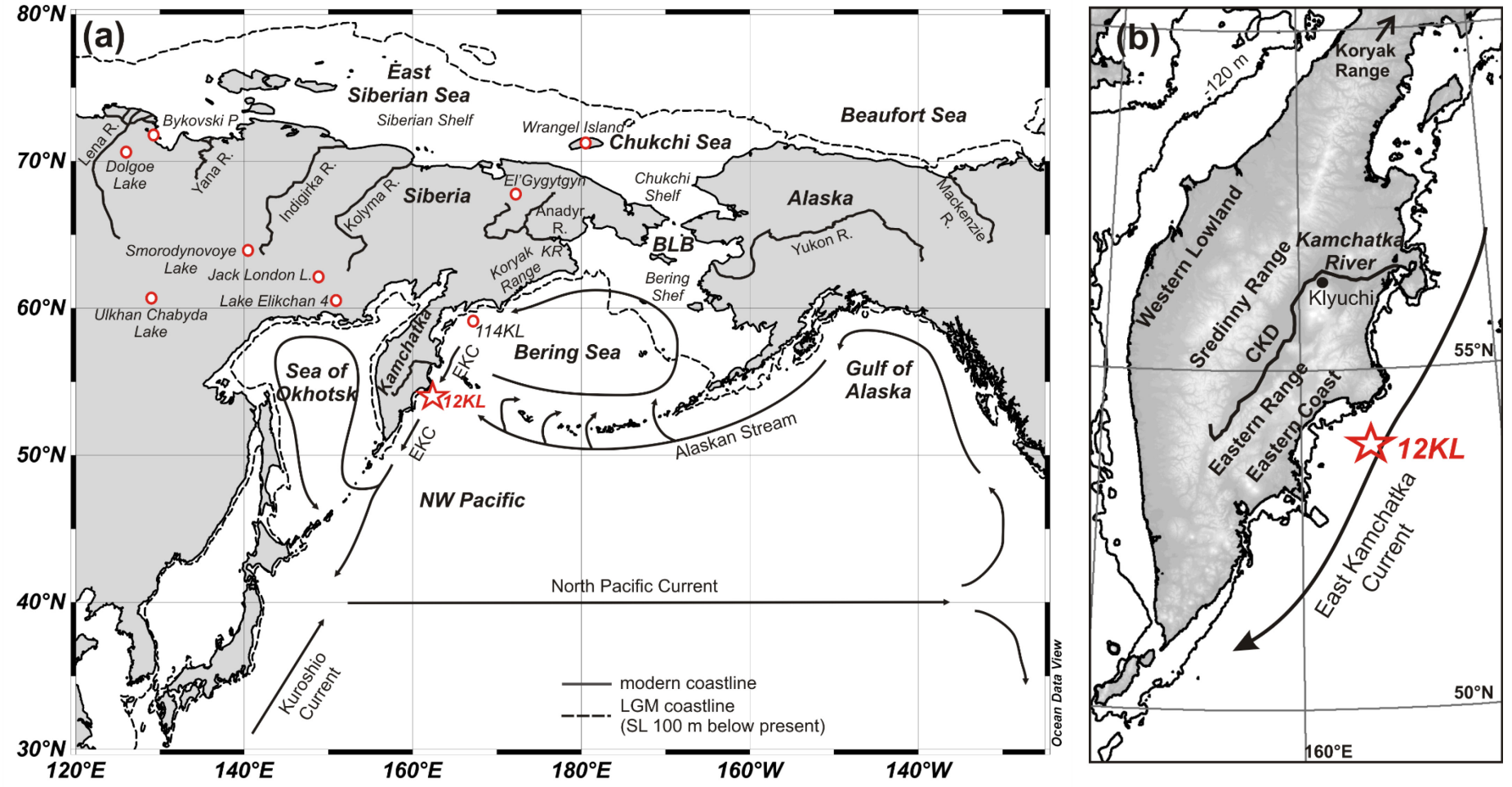
(a)
East Siberian Sea
Siberian Shelf
Beaufort Sea
Wrangel Island
Chukchi Sea
Bykovski P.
Lena R.
Dolgoe Lake
Yana R.
Indigirka R.
Kolyma R.
Siberia
El'Gygytgyn
Anadyr R.
Chukchi Shelf
Alaska
Mackenzie R.
Yukon R.
BLB
Bering Shef
Koryak KR.
Koryak Range
Smorodynovoye Lake
Jack London L.
Lake Elikchan 4
Ulkhan Chabyda Lake
114KL
Bering Sea
Sea of Okhotsk
Kamchatka
EKC
12KL
Gulf of Alaska
Alaskan Stream
NW Pacific
North Pacific Current
Kuroshio Current
modern coastline
LGM coastline
(SL 100 m below present)
Ocean Data View
80°N
70°N
60°N
50°N
40°N
30°N
120°E
140°E
160°E
180°E
160°W
140°W
(b)
120 m
Koryak Range
Western Lowland
Sredinny Range
Kamchatka River
Klyuchi
CKD
Eastern Range
Eastern Coast
12KL
East Kamchatka Current
55°N
50°N
160°E

Fig. 1

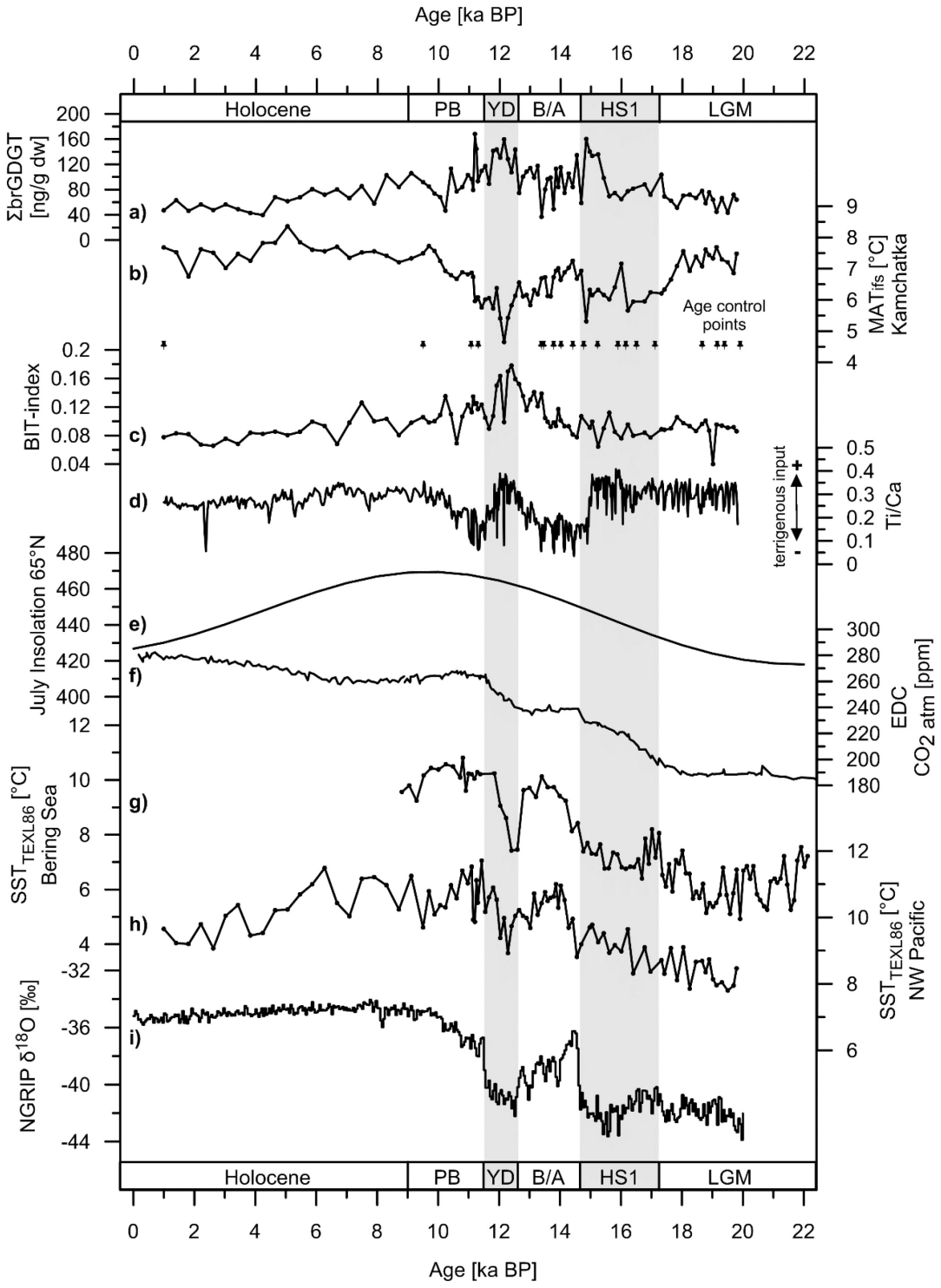
Age [ka BP]
0 2 4 6 8 10 12 14 16 18 20 22
Holocene
PB
YD
B/A
HS1
LGM
ΣbrGDGT [ng/g dw]
200 160 120 80 40 0
a)
b)
MATtfs [°C] Kamchatka
9 8 7 6 5 4
Age control points
BIT-index
0.2 0.16 0.12 0.08 0.04
c)
d)
terrigenous input
+
-
Ti/Ca
0.5 0.4 0.3 0.2 0.1 0
July Insolation 65°N
480 460 440 420 400
e)
f)
EDC CO_2 atm [ppm]
300 280 260 240 220 200 180
SST_{TEXL86} [°C] Bering Sea
12 10 8 6 4
g)
h)
SST_{TEXL86} [°C] NW Pacific
12 10 8 6
NGRIP $\delta^{18}O$ [‰]
-32 -36 -40 -44
i)
Holocene
PB
YD
B/A
HS1
LGM
0 2 4 6 8 10 12 14 16 18 20 22
Age [ka BP]

Fig. 2

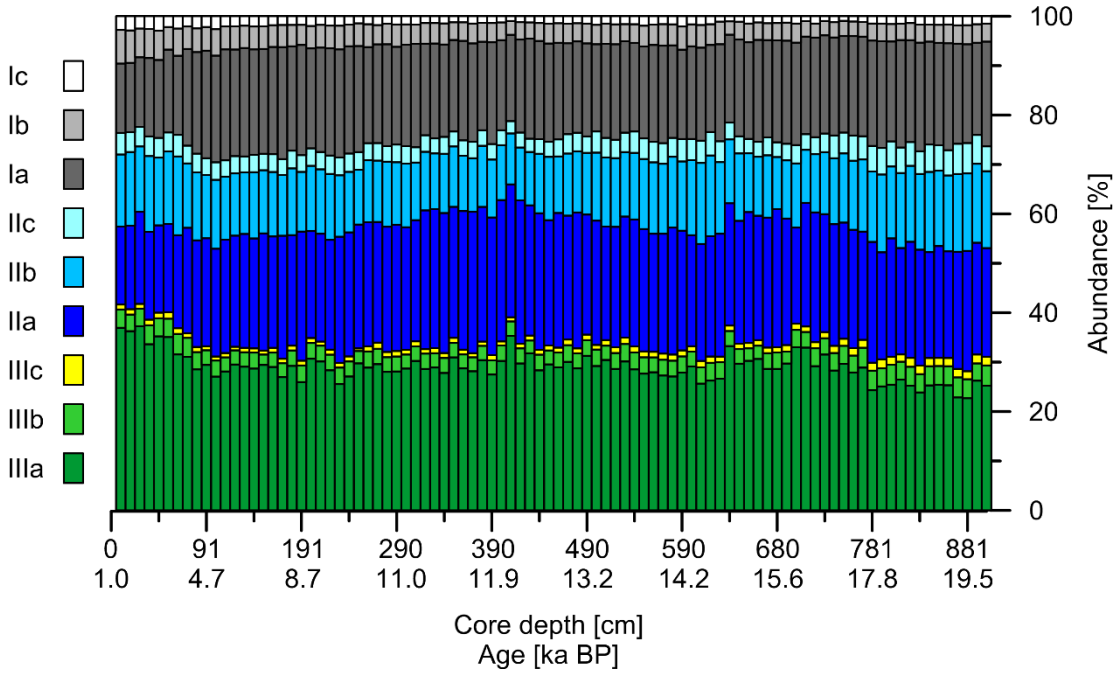
Ic
Ib
Ia
IIc
IIb
IIa
IIIc
IIIb
IIIa
100
80
60
40
20
0
Abundance [%]
0
1.0
91
4.7
191
8.7
290
11.0
390
11.9
490
13.2
590
14.2
680
15.6
781
17.8
881
19.5
Core depth [cm]
Age [ka BP]

Fig. 3

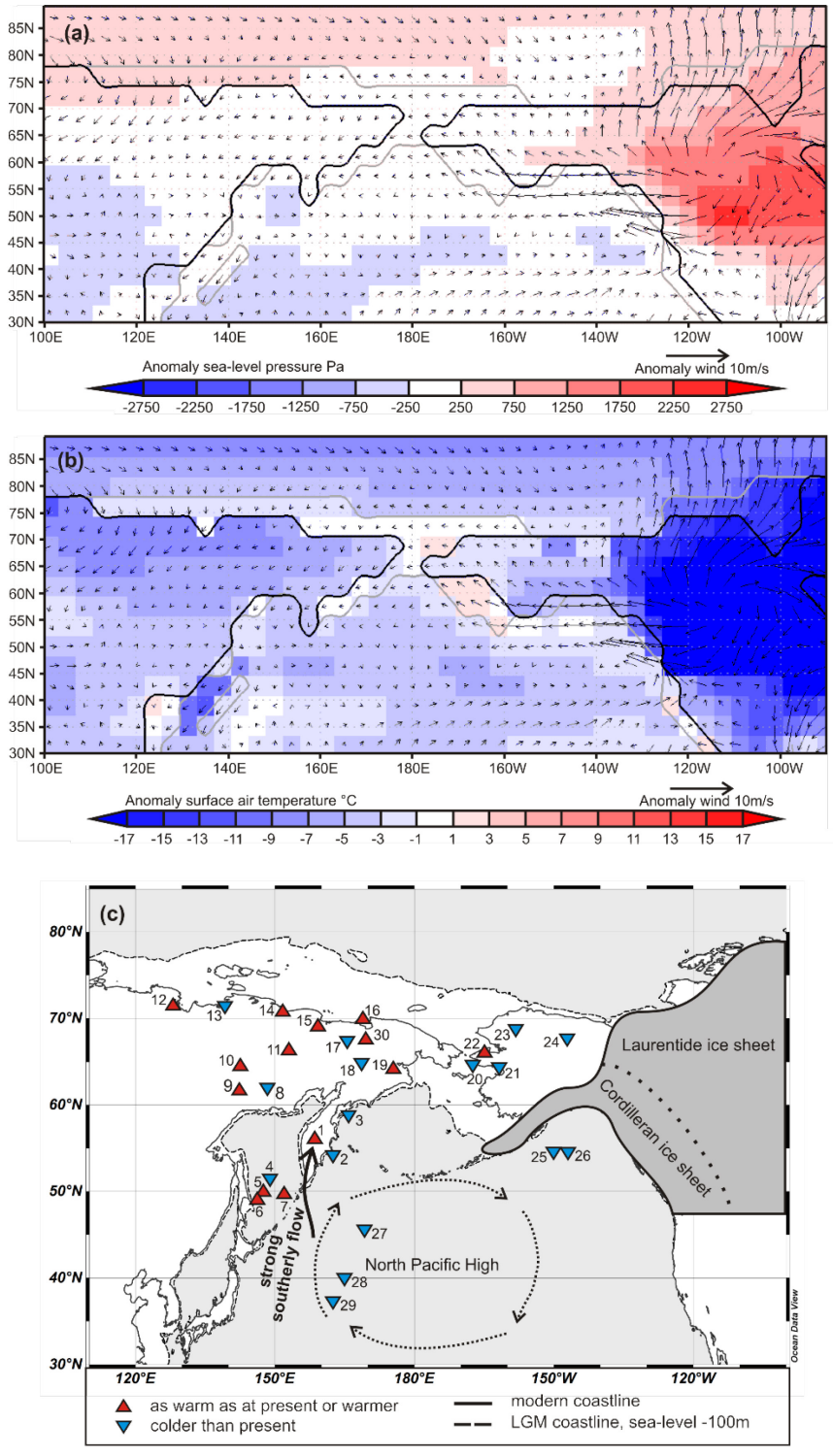
(a)
85N
80N
75N
70N
65N
60N
55N
50N
45N
40N
35N
30N
100E
120E
140E
160E
180E
160W
140W
120W
100W
Anomaly sea-level pressure Pa
Anomaly wind 10m/s
-2750 -2250 -1750 -1250 -750 -250 250 750 1250 1750 2250 2750
(b)
Anomaly surface air temperature °C
Anomaly wind 10m/s
-17 -15 -13 -11 -9 -7 -5 -3 -1 1 3 5 7 9 11 13 15 17
(c)
80°N
70°N
60°N
50°N
40°N
30°N
120°E
150°E
180°E
150°W
120°W
Laurentide ice sheet
Cordilleran ice sheet
North Pacific High
strong southerly flow
as warm as at present or warmer
colder than present
modern coastline
LGM coastline, sea-level -100m
Ocean Data View

Fig. 4

Appendix A

Table A1. Sites and references for the data compiled in Fig. 4c. BLB: Bering Land Bridge.

No.	Site	Region	Proxy	Reference
1	SO201-2-12KL	NW Pacific/Kamchatka	CBT/MBT'	This study
2	SO201-2-12KL	NW Pacific	TEX^{L}_{86}	Meyer et al., 2016
3	SO201-2-114KL	Western Bering Sea	TEX^{L}_{86}	Meyer et al., 2016
4	MR0604-PC7	Sea of Okhotsk	$U^{K'}_{37}$	Seki et al., 2009, 2014
5	XP98-PC2	Sea of Okhotsk	$U^{K'}_{37}$	Seki et al., 2004
6	XP98-PC4	Sea of Okhotsk	$U^{K'}_{37}$	Seki et al., 2004
7	MR00K03-PC04	Sea of Okhotsk	$U^{K'}_{37}$	Harada et al., 2004, 2012
8	unknown	Sosednee Lake/Siberia	pollen	Lozhkin et al., 1993
9	unknown	Oymyakon Depression/Siberia	beetle	Berman et al. (2011)
10	unknown	Middle stream of Indigirka River/Siberia	beetle	Berman et al. (2011)
11	unknown	Lower and middle reaches Kolyma River/Siberia	beetle	Berman et al. (2011)
12	Mkh	Bykovski Peninsula/Siberia	pollen/beetle	Kienast et al. (2005); Sher et al. (2005)
13	YA02-Tums1	Yana lowlands/Siberia	pollen	Pitul'ko et al. (2007)

continued on the next page

14	unknown	Indigirka Lowland/Siberia	beetle	Alfimov and Berman, (2001); Kieselev (1981)
15	unknown	Kolyma Lowland/Siberia	beetle	Alfimov and Berman, (2001); Kieselev (1981)
16	unknown	Ayon Island/Siberia	beetle	Alfimov and Berman, (2001); Kieselev (1981)
17	PG1351	Lake El'Gygytgyn	pollen	Lozhkin et al. (2007)
18	unknown	Markovo/Siberia	beetle	Alfimov and Berman, (2001); Kieselev (1981)
19	unknown	Anadyr River middle stream /Siberia	beetle	Berman et al. (2011);
20	Bering Shelf 78-15	Shelf off Seward Peninsula/BLB	beetle	Elias et al. (1996, 1997); Elias (2001)
21	Zagoskin Lake	western Alaska	chironomids	Kurek et al. (2009)
22	Bering Land Bridge Park	Seward Peninsula/Alaska	beetle	Elias et al. (2001)
23	Burial Lake	St. Michael Island /BLB, Alaska	chironomids	Kurek et al. (2009)
24	Bluefish	Bluefish Basin/Alaska	beetle	Mathews and Telka, (1997); Elias et al. (2001)
25	SO202-27-6	Gulf of Alaska	$U^{K'}_{37}$	Maier et al. (2015)

continued on the next page

26	PAR87A-10	Gulf of Alaska	dinocysts	deVernal and Pedersen (1997)
27	MR97-02 St. 8s	NW Pacific	$U^{K'}_{37}$	Harada et al. (2004, 2012)
28	MR98-05 St. 5	NW Pacific	$U^{K'}_{37}$	Harada et al. (2004, 2012)
29	MR98-05 St. 6	NW Pacific	$U^{K'}_{37}$	Harada et al. (2004, 2012)
30	unknown	Chaun Depression/Siberia	beetle	Berman et al. (2011)